The Dehydratase ADT3 Affects ROS Homeostasis and Cotyledon Development[1][OPEN]

Alessia Para, DurreShahwar Muhammad, Danielle A. Orozco-Nunnelly, Ramis Memishi, Sophie Alvarez, Michael J. Naldrett, and Katherine M. Warpeha*

Weinberg College of Art and Science, Northwestern University, Evanston, Illinois 60208 (A.P.); Department of Biological Sciences, University of Illinois at Chicago, Chicago, Illinois 60607 (D.M., D.A.O.-N., R.M., K.M.W.); and Proteomics and Mass Spectrometry Facility, Donald Danforth Plant Science Center, St. Louis, Missouri 63132 (S.A., M.J.N.)

ORCID IDs: 0000-0003-3381-0504 (D.A.O.-N.); 0000-0001-7662-2437 (R.M.); 0000-0001-8550-2832 (S.A.).

During the transition from seed to seedling, emerging embryos strategically balance available resources between building up defenses against environmental threats and initiating the developmental program that promotes the switch to autotrophy. We present evidence of a critical role for the phenylalanine (Phe) biosynthetic activity of AROGENATE DEHYDRATASE3 (ADT3) in coordinating reactive oxygen species (ROS) homeostasis and cotyledon development in etiolated Arabidopsis (*Arabidopsis thaliana*) seedlings. We show that ADT3 is expressed in the cotyledon and shoot apical meristem, mainly in the cytosol, and that the epidermis of *adt3* cotyledons contains higher levels of ROS. Genome-wide proteomics of the *adt3* mutant revealed a general down-regulation of plastidic proteins and ROS-scavenging enzymes, corroborating the hypothesis that the ADT3 supply of Phe is required to control ROS concentration and distribution to protect cellular components. In addition, loss of ADT3 disrupts cotyledon epidermal patterning by affecting the number and expansion of pavement cells and stomata cell fate specification; we also observed severe alterations in mesophyll cells, which lack oil bodies and normal plastids. Interestingly, up-regulation of the pathway leading to cuticle production is accompanied by an abnormal cuticle structure and/or deposition in the *adt3* mutant. Such impairment results in an increase in cell permeability and provides a link to understand the cell defects in the *adt3* cotyledon epidermis. We suggest an additional role of Phe in supplying nutrients to the young seedling.

During the transition from seed to seedling, the coordination of defense and development is critical for early survival (Finch-Savage and Leubner-Metzger, 2006; Holdsworth et al., 2008). After emerging from the seed coat, the embryo pushes through the soil to reach the surface; at this time, it is more vulnerable to biotic and abiotic stresses (Raven et al., 2005), and underlying actors of this transition are relatively unstudied (Warpeha and Montgomery, 2016). Phe-derived compounds, the phenylpropanoids, play an important role in the first line of defense by contributing to the reinforcement of the external cuticle layer and by conferring UV light protection properties to epicuticular waxes (Steyn et al., 2002; Pollard et al., 2008); in addition, phenylpropanoids influence wax production in response to UV light exposure (Rozema et al., 2002; Pollard et al., 2008; Warpeha et al., 2008). The activity of the phenylpropanoid pathway provides an additional line of defense, as phenolic compounds take part in a nonenzymatic mechanism to efficiently scavenge reactive oxygen species (ROS), whose levels increase as a result of metabolic reactions and when plants initiate a stress response (Sharma et al., 2012; Agati et al., 2013). Moreover, by influencing the cell's ability to balance and modulate ROS production and scavenging, phenylpropanoids allow fluctuations in ROS levels that are required to elicit stress signaling pathways for specific defense strategies (Apel and Hirt, 2004; Mittler et al., 2011).

AROGENATE DEHYDRATASE3 (ADT3)/PREPHENATE DEHYDRATASE1 belongs to the arogenate dehydratase protein family, whose members catalyze the last steps of the biosynthesis of Phe (Warpeha et al., 2006; Cho et al., 2007; Tzin and Galili, 2010; Bross et al., 2011). Activation of ADT3 leads to an increase in Phe content and in the production of phenylpropanoids (Warpeha et al., 2006). Accordingly, loss of ADT3 results in an enhanced sensitivity to UV irradiation in etiolated

[1] This work was supported by the National Science Foundation (grant no. MCB–0848113 to K.M.W. and Lon S. Kaufman).

* Address correspondence to kwarpeha@uic.edu.

The author responsible for distribution of materials integral to the findings presented in this article in accordance with the policy described in the Instructions for Authors (www.plantphysiol.org) is: Katherine M. Warpeha (kwarpeha@uic.edu).

Original project was conceived by K.M.W.; K.M.W. supervised the experiments; K.M.W. performed laboratory experiments (except proteome) with technical assistance from D.M., D.A.O.-N., and R.M., with S.A. and M.J.N. conducting the proteome on K.M.W. samples, and A.P. handling data analysis of all proteomic data; K.M.W. designed the experiments with input from the other authors, especially A.P.; A.P. and K.M.W. analyzed the data; A.P. wrote the article with input on proteome from S.A. and M.J.N., with editing and oversight from K.M.W.

[OPEN] Articles can be viewed without a subscription.

www.plantphysiol.org/cgi/doi/10.1104/pp.16.00464

 © 2016 American Society of Plant Biologists. All Rights Reserved.

seedlings due to the reduced synthesis of photoprotective compounds and UV light-scattering epicuticular waxes (Warpeha et al., 2008). However, the physiological and molecular bases of this phenotype and the function of ADT3 in the seed-to-seedling transition remain to be elucidated.

We sought to understand the role of ADT3 post-germination, in the seed-to-seedling transition. ADT3 is expressed early in seedling growth (Warpeha et al., 2006; Hruz et al., 2008). Localization studies in Arabidopsis (*Arabidopsis thaliana*) using protoplasts from cell suspension and light-grown rosette leaves have placed this enzyme within the chloroplast (Rippert et al., 2009), while we have reported ADT3 activity in the cytosolic fraction in young etiolated seedlings (Warpeha et al., 2006). These reports differ likely due to the different age and growth conditions of the studied plant material. Cytosolic forms of chorismate mutase, which act at the first committed step in the Phe and Tyr biosynthesis pathway, were found in Arabidopsis and other plants (d'Amato et al., 1984; Benesova and Bode, 1992; Eberhard et al., 1996), suggesting the possibility of extraplastidic Phe biosynthesis.

Here, we report in transgenic complementation experiments that ADT3 is expressed widely in the young shoot and largely accumulates in the cytosol. Based on the role of phenylpropanoids in plant defense, we hypothesize that the ADT3 regulation of Phe supply is required to coordinate defense and development at the seed-to-seedling transition. We found that, without ADT3, the cells of the epidermis cannot buffer and restrict ROS; moreover, *adt3* cotyledons enter an aberrant developmental program that results in abnormal morphology and patterning as well as several alterations at the subcellular level. Proteomic analysis of *adt3* seedlings provided insights into the molecular basis of *adt3* phenotypes, as it uncovered a chronic inability to buffer an excess of ROS and maintain plastid integrity. It also revealed a failed attempt to control cell rheology through up-regulation of the biochemical pathway for cuticle biosynthesis and assembly, as indicated by the increase in the permeability of *adt3* epidermal cells; we propose that this also could be the cause of the defecting epidermal patterning in *adt3* cotyledons. In addition, we suggest an additional role of Phe in nutrient supply in etiolated seedlings.

RESULTS

ADT3 Is Expressed in Cotyledons of Young Etiolated Seedlings, Where Its Loss Causes an Imbalance in ROS Homeostasis

To investigate the impact of the loss of ADT3, we generated transgenic plants where native ADT3 fused to cyan fluorescent protein (CFP) was driven by its native promoter (*ADT3*::ADT3-CFP) in the *adt3-1* mutant background to examine the ADT3 spatial expression pattern in 4-d-old dark-grown seedlings (Fig. 1). ADT3 is expressed in the shoot in developing mesophyll and in shoot apical meristem (SAM [leaf primordia and dome]; Fig. 1A) and epidermal cells, especially pavement cells (Fig. 1B). In particular, ADT3 appeared to accumulate mainly in the cytosol (Fig. 1, insets). An additional transgenic line harboring the *ADT3*::ADT3-GFP fusion in the *adt3-1* mutant background recapitulated the *ADT3*::ADT3-CFP expression pattern and showed complementation of all *adt3* defects reported herein (Supplemental Fig. S1; see below) and elsewhere (Warpeha et al., 2008). A similar expression pattern of *ADT3*::ADT3-GFP was observed in the wild-type background, where a more intense GFP signal was observed compared with the mutant background. ADT3 expression also was observed in the developing guard cells (Supplemental Fig. S2).

The *adt3* mutation has been shown previously to make etiolated seedlings vulnerable to UV irradiation, and the defect was proposed to be due to a decrease in the production of phenylpropanoids upon exposure to both blue light and UV light (Warpeha et al., 2006, 2008). To elucidate the physiological basis of UV light sensitivity in relation to phenylpropanoids, we examined the accumulation of ROS in the epidermis of *adt3-1* cotyledons before and after UV light treatment, as these compounds are produced in response to short-wavelength light (Wituszyńska and Karpiński, 2013; Consentino et al., 2015). Six-day-old dark-grown wild-type and *adt3-1* seedlings were irradiated with a sublethal dose of UV-C radiation, and the CellRox Deep Red cell-permeable fluorescent probe was used to detect ROS (Fig. 2). This probe only fluoresces when in contact with ROS, and the signal can be captured when excited by the Cy5 light-emitting diode (LED; false-colored pink).

Interestingly, probe fluorescence in the epidermis was detected in dark-grown unirradiated *adt3-1* compared with unirradiated wild-type (control) seedlings, indicating that basal ROS levels are elevated in *adt3-1* (Fig. 2). Irradiation with a sublethal UV-C light dose caused an increase in CellRox basal signal from both wild-type and *adt3-1* pavement cells (Fig. 2, bar graph). An additional *ADT3* mutant (*adt3-6*) tested responded similarly to *adt3-1* (Supplemental Fig. S3). Since ADT3 catalyzes the last step of the biosynthesis of Phe (Maeda and Dudareva, 2012), we assessed the requirement of Phe in counteracting ROS by transferring living, whole 6-d-old wild-type, *adt3-1*, and *adt3-6* seedlings to Phe-supplemented medium for 3 h before subjecting them to a sublethal dose of UV-C radiation, immediately followed by incubation with CellRox, where pre-incubation with Phe restored the seedling to control (wild-type unirradiated) levels of ROS in both *adt3* alleles (Fig. 2; Supplemental Fig. S3). Another probe for ROS detection, Singlet Oxygen Sensor Green (SOSG), indicated similar results for *adt3-1* compared with the wild type, confirming that ROS production is elevated significantly as a consequence of the loss of *ADT3* (Supplemental Fig. S4), whereas *adt3-6* ROS production was not elevated significantly.

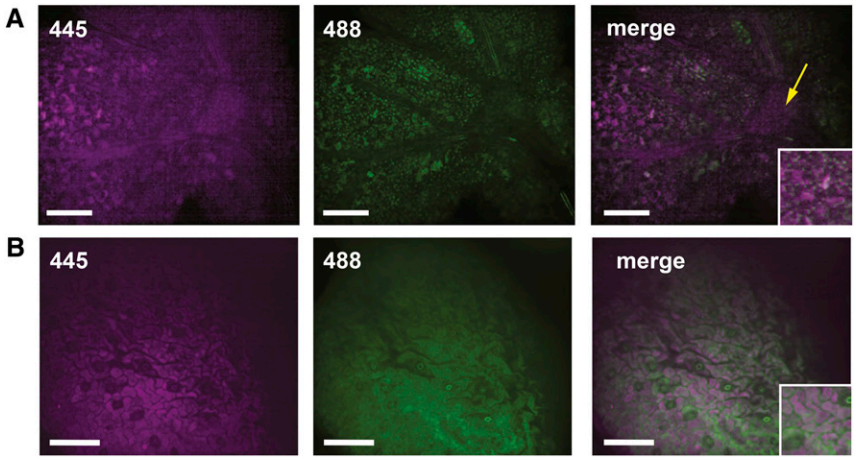

Figure 1. ADT3 localizes predominantly in the cotyledon of young, dark-grown seedlings. The expression of *ADT3*::ADT3-CFP was analyzed in live 4-d-old *adt3* seedlings by spinning disk confocal microscopy. A, In this view, CFP fluorescence (445 nm; false-colored magenta) is detected in developing mesophyll cells of the cotyledon and in the SAM (yellow arrow; 1-μm-thick optical slice). Autofluorescence from developing plastids (488 nm; false-colored green) is visible. Merged images of 445 and 488 nm indicate that ADT3 localizes mainly in the cytosol. B, In the epidermal layer view, *ADT3*::ADT3-CFP accumulates in the pavement cells and young guard cell lineage but not in mature guard cells. The signal captured by 488 nm is due to the accumulation of polyphenol (flavonoid) autofluorescence in the epidermis. Images are representative, 60×; $n = 20$. Bars = 50 μm.

To test whether Phe metabolism is required to scavenge ROS, we UV-C irradiated 6-d-old, dark-grown seedlings of the *fah1-7/tt4-1* double mutant (Li et al., 1993; Landry et al., 1995; Peer et al., 2001), which cannot metabolize Phe to produce flavonoids. Indeed, we observed that pretreatment with Phe was able to prevent UV light-induced ROS production in the *fah1-7/tt4-1* background (Supplemental Fig. S3). Accordingly, pretreatment with Phe had the same effect as potassium iodide, a known ROS scavenger (Tsukagoshi et al., 2010), which also was able to prevent a ROS increase upon UV-C irradiation (Supplemental Fig. S5). Likewise, treatment with a nonmetabolizable Phe analog, p-f-DL-Phe (Conway et al., 1963), caused a significant decrease in Cy5 fluorescence in UV-C-irradiated pavement cells (but not in guard cells) in the *adt3-1* epidermis (Supplemental Fig. S5). Taken together, these results indicate that ROS homeostasis is altered in dark-grown *adt3* seedlings. In addition, we observed that Phe per se could prevent significant ROS accumulation as a result of UV-C irradiation.

Loss of ADT3 Disturbs Epidermis Development in the Cotyledons of Dark-Grown Seedlings

To further investigate the consequences of the loss of ADT3, we examined the cellular makeup of the cotyledon's epidermis. DAPI illumination of the epidermis of live 6-d-old dark-grown wild-type and *adt3-1* seedlings enabled a clear distinction of cell lineages (pavement cells largely reflect, and guard cells largely absorb, DAPI) and revealed that *adt3-1* mutants produced fewer but larger pavement cells than the wild type (Fig. 3A); however, *adt3-1* cotyledons are wider than wild-type cotyledons (Fig. 3). In addition, a reduced number of guard cells was observed for the *adt3* mutant cotyledons (Fig. 3). Addition of Phe to the growth medium from sowing rescued both the pavement cell and guard cell phenotypes in *adt3-1* mutants (Fig. 3). *adt3-6* seedlings also presented similar phenotypes, which could be rescued by Phe (Supplemental Fig. S6A). The defects persisted when exogenous L-Tyr or L-Trp (which derive from the shikimate pathway like Phe) was supplied instead of Phe (Supplemental Fig. S7).

To address whether the guard cell defect was due to failure to specify the stomatal lineage, we supplied Phe to the mutants *speechless* and *mute*, which disrupt early and late steps of the stomata lineage progression, respectively (MacAlister et al., 2007; Pillitteri et al., 2007). Phe did not prevent the guard cell defects in these mutants, indicating that Phe is required upstream of these guard cell specification factors (Supplemental Fig. S7).

In summary, we observed ADT3 expression in the cytoplasm of epidermal cells of the cotyledons and of the SAM. Loss of *ADT3* severely affects the number and morphogenesis of pavement cells and disrupts guard cell development. The defects were rescued by supplementing Phe but not other amino acids, indicating that the metabolism of ADT3-supplied Phe impacts cotyledon patterning in etiolated seedlings.

adt3 Cotyledons Exhibit Abnormal Subcellular Features

We also examined the ultrastructure of the epidermis and mesophyll cells in cotyledons of 6-d-old, dark-grown *adt3-1* seedlings by transmission electron microscopy (TEM; Fig. 4A). A prominent feature

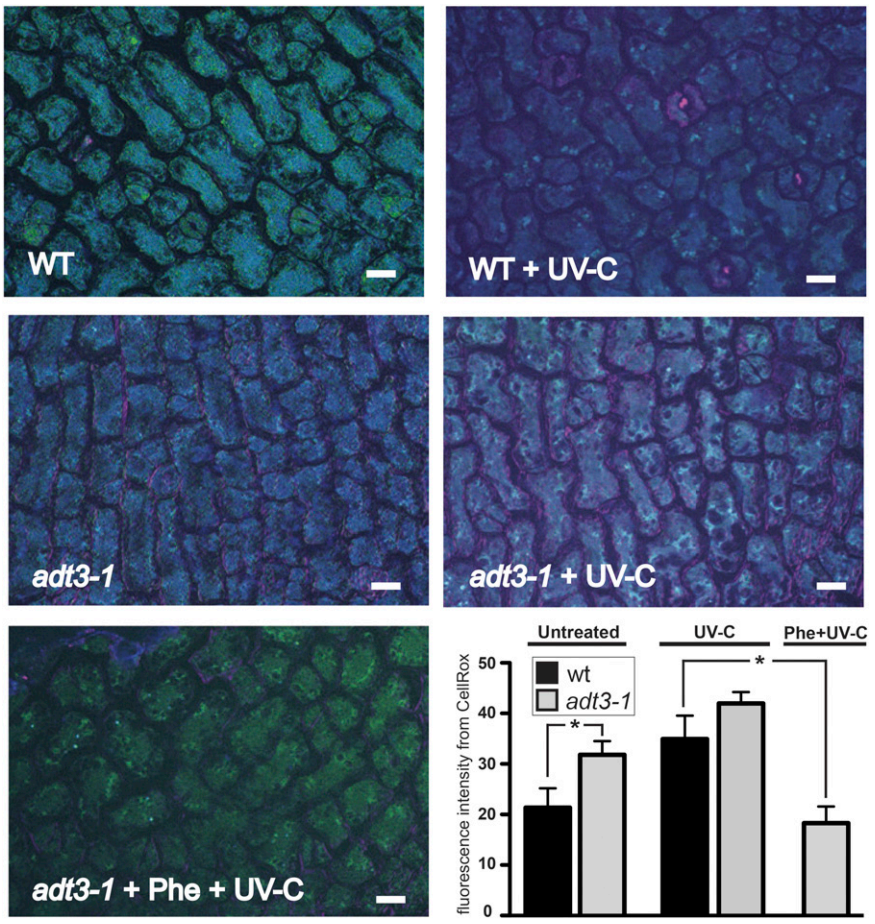

Figure 2. ROS levels are elevated in *adt3* mutant seedlings compared with the wild type. The cotyledon epidermis cells of live 6-d-old dark-grown seedlings incubated with CellRox Deep Red cell-permeable fluorescent dye are shown (merged 4′,6-diamino-phenylindole [DAPI], fluorescein isothiocyanate [FITC], and Cy5). Wild-type (WT; top) and *adt3-1* (middle) seedlings were either mock irradiated (unirradiated control; left) or irradiated with 254 nm (+ UV-C; right), then immediately immersed in CellRox reagent, which emits fluorescence in Cy5 in the presence of ROS. *adt3-1* also was treated with 500 μM Phe (+ Phe) for 3 h and then irradiated with 254 nm (+ UV-C; bottom left). After washes and mounting in sterile water, seedlings were imaged at 1-μm optical slice thickness on a deconvoluting microscope in the epidermal plane. CellRox signal is low in untreated wild-type cells and increases as a result of UV-C irradiation, while signal is evident in unirradiated *adt3-1* cells. Feeding Phe to *adt3-1* seedlings before irradiation prevented ROS accumulation (bottom left). Bars = 10 μm. In the bar graph at bottom right, Cy5 fluorescence from excited CellRox (false-colored pink) was quantified in pavement cells (relative fluorescence; i.e. artificial units). Each value represents a minimum of six cells of four replicates, with a minimum of 20 representative seedlings viewed per replicate. Error bars represent SE. *, $P < 0.05$.

we observed was the reduction in the number of globular oil bodies in *adt3-1* mesophyll cells compared with the wild type (Fig. 4A, insets c and f). In addition, *adt3-1* cells were hypervacuolated (especially the epidermis), while most wild-type cells contained a large central vacuole (Fig. 4A). Developing plastids were identified in the wild type, as they stain densely and contain prolamellar bodies with stromal strands extending from the thylakoid membrane (Fig. 4A, inset b), whereas the *adt3-1* plastids displayed atypical prolamellar bodies and loose stromal thylakoids (Fig. 4A, inset e). The cytoplasm of *adt3-1* epidermal cells had a blackened appearance, indicating a possible accumulation of osmiophilic material, and exhibited numerous round organelles, which are likely to be mitochondria, as suggested by the ribbed structure (Fig. 4A, insets a and c).

The distribution of oil bodies in the wild type and *adt3-1* was further investigated using the lipophilic stain Nile Red (Greenspan et al., 1985). Optical sections of *adt3* cotyledons showed a paucity of scattered oil bodies (Fig. 4B), while in the wild type, these organelles were more abundant, particularly at the tip (Fig. 4B). Addition of Phe to the germination medium increased oil body production in *adt3-1* (Fig. 4B), rescuing the deficiency. This phenotype also was observed for the *adt3-6* allele (Supplemental Fig. S6). Thus, ADT3 activity is required to preserve the subcellular structure of the cells of the cotyledons in etiolated seedlings.

The *adt3* Proteome Reveals the Molecular Basis of the *adt3* Mutant Phenotypes

In order to uncover the molecular phenotype underlying the *adt3* phenotypes, we obtained a comparative protein expression profile of the aerial portions (upper hypocotyl and cotyledon) of *adt3-1* and wild-type seedlings. We used the bioinformatics platform Virtual Plant for Gene Ontology (GO) term analyses (Katari et al., 2010) and the Kyoto Encyclopedia of Genes and Genomes (KEGG) database for metabolic pathways (http://www.genome.jp/kegg/).

The proteomic analysis revealed that *adt3-1* mutation caused alteration of the expression of 1,333 proteins, 608 of which were down-regulated and 725 of which were up-regulated (Supplemental Table S1). The maximum fold change was 1.69 for up-regulation and 0.646 for down-regulation, a dynamic range of expression in accordance with other proteomics studies (Supplemental Table S1; Alvarez et al., 2011, 2014).

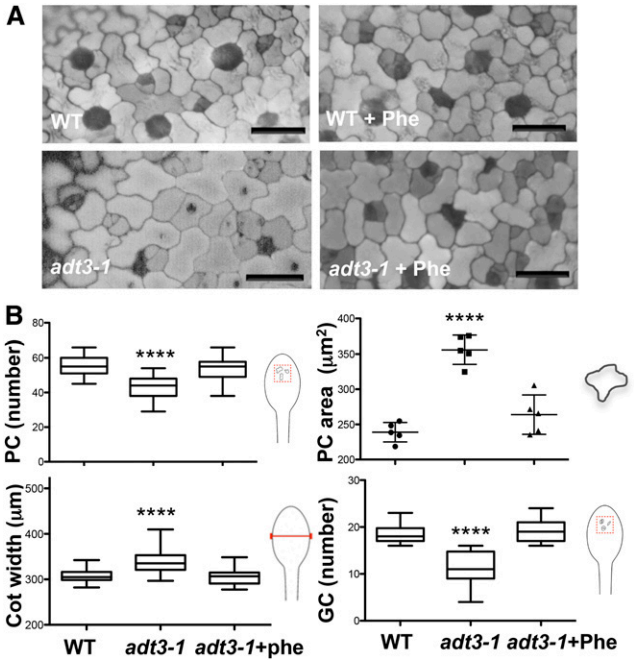

Figure 3. Epidermal defects of *adt3-1* seedlings. A, Epidermis of wild-type (WT; top) and *adt3-1* (bottom) live cotyledons viewed on a deconvoluting microscope (DAPI contrast). Guard cell lineage (meristemoid and guard cells) cells appear dark gray, and pavement cells appear light gray. Defects are prevented by the inclusion of Phe in the medium (right images). Bars = 25 μm. B, Measurement of pavement cell (PC) area and number, cotyledon (Cot) width, and guard cell (GC) number in the wild type and *adt3-1* without and with added Phe. Cartoons indicate the structures measured. Error bars represent SE. ****, $P < 0.0001$. $n = 4$ replicates (20–40 seedlings per experimental condition).

Given the high number of statistically significantly misregulated proteins in the *adt3-1* proteome, we investigated whether small changes in expression could be biologically significant by asking whether they occur in a specific tissue or at multiple steps within the same process, as conceptualized by metabolic control analysis (Kacser and Burns, 1995; Fell and Cornish-Bowden, 1997). First, we queried the Plant Ontology (PO) database in Virtual Plant to assess the enrichment of proteins of different cell and organ types. For both *adt3-1* up-regulated and down-regulated proteins, the most significant PO enrichment was observed for guard cell, shoot epidermal cell, and epidermal cell (Table I), indicating that the changes in protein expression were relevant to the cell types of the cotyledons where we observed ADT3 expression (Fig. 1A). Next, plant-specific overrepresented terms for cellular compartment, molecular function, and biological process were assessed by GO term analysis using a *P* value of 0.01 as the cutoff. The results of this analysis are summarized in Tables I and II and Supplemental Tables S2 to S11.

GO term analysis of up-regulated proteins in the *adt3-1* proteome revealed enrichment for plasma membrane and vacuole factors involved in transport as well as in cell wall organization or biogenesis through the metabolism of the polysaccharides xylan and glucan (Table I). Accordingly, the most represented molecular function for the cell wall category is hydrolase activity, since in these polymers the monosaccharide residues are joined by glycosidic linkages. The involvement of the cell wall in *adt3* cell morphology is also underscored by the GO term growth, which showed one of the most significant enrichments for the up-regulated proteins in the *adt3-1* proteome (Table I). The proteins belonging to this category are involved in cell expansion, like expansins (EXP3, EXP9, EXP11, and EXPL1) and DIM1 (Takahashi et al., 1995). Interestingly, a protein that showed the highest increase in the *adt3-1* mutant is AT14A, which was shown to function like integrin in animals to regulate cell shape and cell-to-cell adhesion (Lü et al., 2012; Supplemental Table S1).

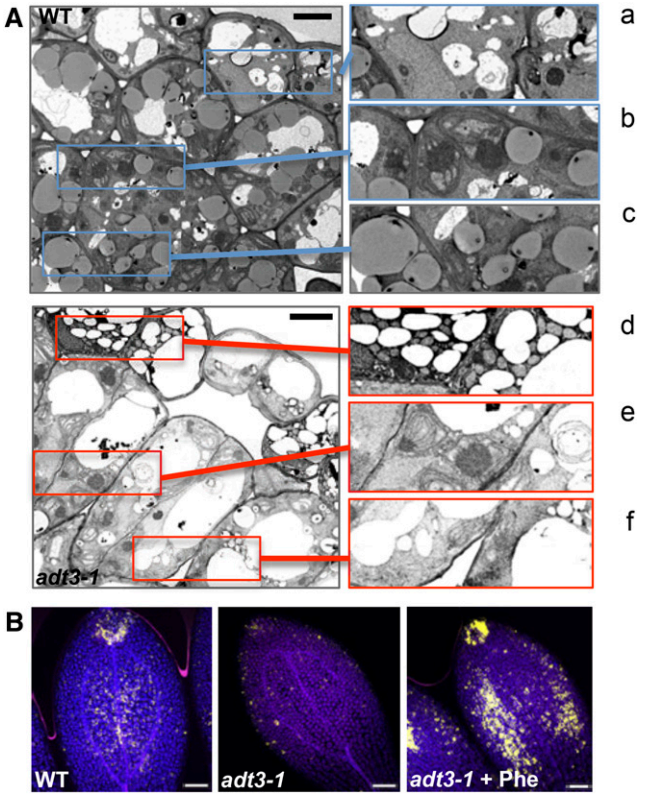

Figure 4. Ultrastructural phenotypes of *adt3-1* epidermal and mesophyll cells. A, TEM micrographs (left) of sections perpendicular to the adaxial surface of the cotyledons of 6-d-old, dark-grown wild-type (WT; top) and *adt3-1* (bottom) seedlings. Details of wild-type (a–c) and *adt3-1* (d–f) micrographs are shown at right: cytoplasm of epidermal cells (a and c), plastids (b and e), and cytoplasm of mesophyll cells (note the absence of oil bodies in f). $n = 5$ seedlings (approximately 100 cells). Bars = 5 μm. B, Adaxial side view of mesophyll cells in the cotyledons of 6-d-old, dark-grown wild-type (left), *adt3-1* (middle), and *adt3-1* + Phe (right) seedlings after staining with Nile Red (false-colored gold). Merges of DAPI (blue), FITC (gold), and Cy5 (pink) are shown. $n = 3$ (30 seedlings). Bars = 50 μm.

Table I. *GO term and PO term analysis of up-regulated and down-regulated proteins in the adt3 proteome*

Term	*P*
Up-regulated proteins in the *adt3* mutant	
PO term	
Guard cell	1.28×10^{-78}
Shoot epidermal cell	2.08×10^{-77}
Epidermal cell	1.33×10^{-76}
Transport	1.17×10^{-16}
Carboxylic acid/oxoacid metabolic process	6.54×10^{-10}
Fatty acid metabolic process	3.42×10^{-06}
GO term	
Plasma membrane	5.70×10^{-109}
Transport	5.92×10^{-27}
Vacuole	2.05×10^{-34}
Transport	2.03×10^{-15}
Cell wall	7.98×10^{-32}
Cell wall organization or biogenesis	3.76×10^{-06}
Xylan catabolic process	1.18×10^{-3}
Glucan metabolic process	4.37×10^{-3}
Hydrolase activity	5.39×10^{-14}
Growth	2.78×10^{-11}
Primary metabolic process	1.94×10^{-14}
Down-regulated proteins in the *adt3* mutant	
PO term	
Shoot epidermal cell	1.19×10^{-86}
Guard cell	4.38×10^{-86}
Epidermal cell	3.35×10^{-84}
Oxidoreductase activity	1.92×10^{-14}
GO term	
Plastid	5.61×10^{-128}
Plastid stroma	6.38×10^{-127}
Envelope	2.77×10^{-50}
Thylakoid	6.28×10^{-46}
Stromule	1.18×10^{-19}
Plastoglobule	3.15×10^{-10}
Nitrogen compound metabolic process	1.8×10^{-17}
Primary metabolic process	7.25×10^{-25}

For *adt3-1* up-regulated proteins assigned to epidermal cells according to the PO database, we noticed an enrichment in proteins involved in carboxylic acid/oxoacid metabolic process (Table I), encompassing enzymes for fatty acid conjugation (LACS4, LACS8, GPAT8, and GPAT4) and the synthesis and elongation of very-long-chain fatty acids (VLCFAs; ACC1/PAS3, CER2, CER6, CER10, ATT1 [CYP86A2], and FDH [KCS10]). We also found up-regulation of the 3-ketoacyl-CoA synthases (KCS) KCS8, KCS9, KCS16, KCS19, and CY86A4 as well as transporters of wax molecules and cuticle building blocks (ABCG11/DSO/CER5 and LTPG1). All of these functions were associated previously with cuticle formation (Kunst and Samuels, 2009; Nawrath et al., 2013, and refs. therein).

When considering down-regulated proteins, one of the most significant GO terms for cellular components is plastid, and the affected proteins are associated with the stroma, envelope, and thylakoid membrane (Table I). This is in agreement with the observation that the integrity of the plastids is compromised by the loss of ADT3 (Fig. 4A). Interestingly, we observed an overrepresentation of proteins associated with the stromule, an elusive plastidic structure that has been implicated previously in GPA1 signaling (Huang et al., 2006; Hanson and Sattarzadeh, 2011; Table I).

One of the top GO terms that describes the overrepresented molecular functions for the group of down-regulated proteins in the epidermis of the *adt3-1* mutant is oxidoreductase activity (Table I), which includes proteins of both the enzymatic and nonenzymatic scavenging system that controls ROS homeostasis, like superoxide dismutases (MSD1, FSD2, CSD2, and CSD3), catalases (CAT2), enzymes of ascorbate-glutathione (AsA-GSH) cycle ascorbate peroxidase (SAPX, APX1, and APX3), monodehydroascorbate reductase (MDAR4), dehydroascorbate reductase (DHAR2), and glutathione reductase (ATGR2; Sharma et al., 2012). GDP-Man 3′,5′-epimerase, an important enzyme in the ascorbate biosynthetic pathway, also is down-regulated (Wheeler et al., 1998). In addition, of the 93 down-regulated proteins that were assigned to gene families, seven are members of the glutathione *S*-transferase family of proteins in *adt3-1* (Supplemental Table S1).

In addition to the GO terms listed above, primary metabolic process is highly significant for both up-regulated and down-regulated proteins in the *adt3-1* proteome (Table I). Hence, we investigated the metabolic pathways that were affected by the loss of ADT3 using the KEGG database. We observed the down-regulation of key enzymes of the central carbohydrate and energy metabolism (Table II), including enzymes of the glycolysis/gluconeogenesis pathway, the pentose phosphate pathway, and glyoxylate and dicarboxylate metabolism. However, some of the enzymes involved in oxidative phosphorylation are up-regulated, suggesting an intense mitochondrial activity. Also, the expression of proteins of starch and Suc metabolism, pentose and glucuronate interconversions, as well as amino sugar and nucleotide sugar metabolism is increased in the *adt3-1* mutant. The enrichment of enzymes from these pathways provides a link between cell wall metabolism and central plant metabolism (Seifert, 2004; Bar-Peled and O'Neill, 2011).

In summary, the overrepresentation of terms for specific biological functions, localization, or molecular components is consistent with the observed *adt3* phenotypes, linking the physiological and morphological alterations to changes in the expression of key proteins or pathways. Moreover, in agreement with functional enrichment analysis, the pathway analysis suggests that alteration of cell morphology and subcellular structure might be linked to metabolic deficiencies as a result of the loss of ADT3 activity.

Cuticle Formation and Cell Permeability Are Altered in *adt3* Cells

Many key proteins involved in the production of the cuticle were up-regulated in the *adt3-1* mutant (Table I;

Table II. *KEGG pathway analysis for up- and down-regulated proteins in the adt3 mutant*

Term	No. of Genes		
	Total[a]	Down-Regulated	Up-Regulated
Carbohydrate metabolism			
Glycolysis/gluconeogenesis	29	19	10
Pyruvate metabolism	27	14	13
Starch and Suc metabolism	27	6	21
Glyoxylate and dicarboxylate metabolism	26	23	3
Amino sugar and nucleotide sugar metabolism	19	4	15
Ascorbate and aldarate metabolism	15	7	8
Pentose and glucuronate interconversions	15	2	13
Citrate cycle (tricarboxylic acid)	14	9	5
Pentose phosphate pathway	11	10	1
Fru and Man metabolism	11	7	4
Inositol phosphate metabolism	7	2	5
Gal metabolism	6	1	5
Energy metabolism			
Carbon fixation in photosynthetic organisms	32	27	5
Oxidative phosphorylation (ATP synthase)	17	6	11
Photosynthesis	11	10	1
Nitrogen metabolism	9	8	1
Sulfur metabolism	6	6	0

[a]Number of input genes assigned by the KEGG database.

Supplemental Table S3). Higher magnification of the outermost cell wall revealed irregular deposition of electron-opaque material within the deeper layers (Fig. 5A), indicating that cuticle biosynthesis and/or deposition is somehow defective. To further examine *adt3-1* cuticular properties, we tested the permeability of *adt3-1* cuticle under hyposmotic conditions using Toluidine Blue (TB) staining (Tanaka et al., 2004). Interestingly, diffuse TB staining was observed in *adt3* seedlings after a 48-h incubation in water (Fig. 5B) compared with the wild type in the same conditions, a sign of incomplete or reduced cuticle in the mutant. TB staining of *adt3-6* dark-grown seedlings showed similar results (data not shown). Since it was found that mutations in genes of the wax biosynthetic pathway that affect the composition of the epicuticular waxes also perturb stomatal development and increase the number of guard cells (Gray et al., 2000; Guseman et al., 2010), we inspected the epidermis of white light-grown *adt3* seedlings and found adjacent stomata that were breaking the one-cell spacing rule (Fig. 5C). Our results indicate that the cuticle of *adt3* epidermis does not achieve a proper organization, and this causes a reduction in the isolating properties of the epidermis and is likely to impact the cell patterning of *adt3* cotyledons.

Suc Supply Restores Guard Cell Number While Asn and NH_4Ac Rescue Pavement Cell Morphology in *adt3* Cotyledons

Proteomic analysis revealed that a significant number of proteins from primary metabolic pathways, in particular for carbon metabolism, are down-regulated in *adt3-1* seedlings (Tables I and II), so we investigated whether carbon input could alleviate the defects in *adt3-1* cotyledons by transferring 4-d-old *adt3-1* seedlings to medium containing 1% Suc. When we examined *adt3-1* cotyledons 48 h later, we found that the pavement cell phenotype was not rescued by exogenous Suc (Fig. 6A); however, the number of guard cells was similar to that in the wild type (Fig. 6A). The rescue was not due to a change in osmotic potential, as it was not ameliorated by exogenous supply of 1% mannitol (Supplemental Fig. S8).

Since ASPARAGINE SYNTHASE1 (ASN1) is up-regulated in the *adt3-1* mutant (Supplemental Table S1), we next attempted to rescue the *adt3-1* phenotype by supplying exogenous Asn at sowing. After 6 d of growth on Asn in darkness, we observed that the pavement cell size and number as well as the cotyledon size were completely restored in the mutant (Fig. 6B). The same results were obtained when ammonium acetate (NH_4Ac) was added to the medium (Fig. 6C). However, the guard cell lineage defect was not corrected by the application of either exogenous Asn or NH_4Ac (Fig. 6, B and C). To test whether the ability of Asn and NH_4Ac to rescue the *adt3-1* cell morphology phenotype could be linked to restored fatty acid production (Fig. 4B), we incubated Asn- and NH_4Ac-supplied *adt3-1* seedlings with Nile Red (Fig. 6C); similar to the result we obtained by supplying Phe (Fig. 4B), addition of Asn and NH_4Ac also resulted in an increase in Nile Red signal (Fig. 6C), indicating that these compounds could be used by *adt3* to feed metabolic pathways that lead to fatty acid production. These observations suggest that a nutrient imbalance could be part of the defects in cell morphology and epidermal patterning of *adt3* cotyledons (Fig. 3).

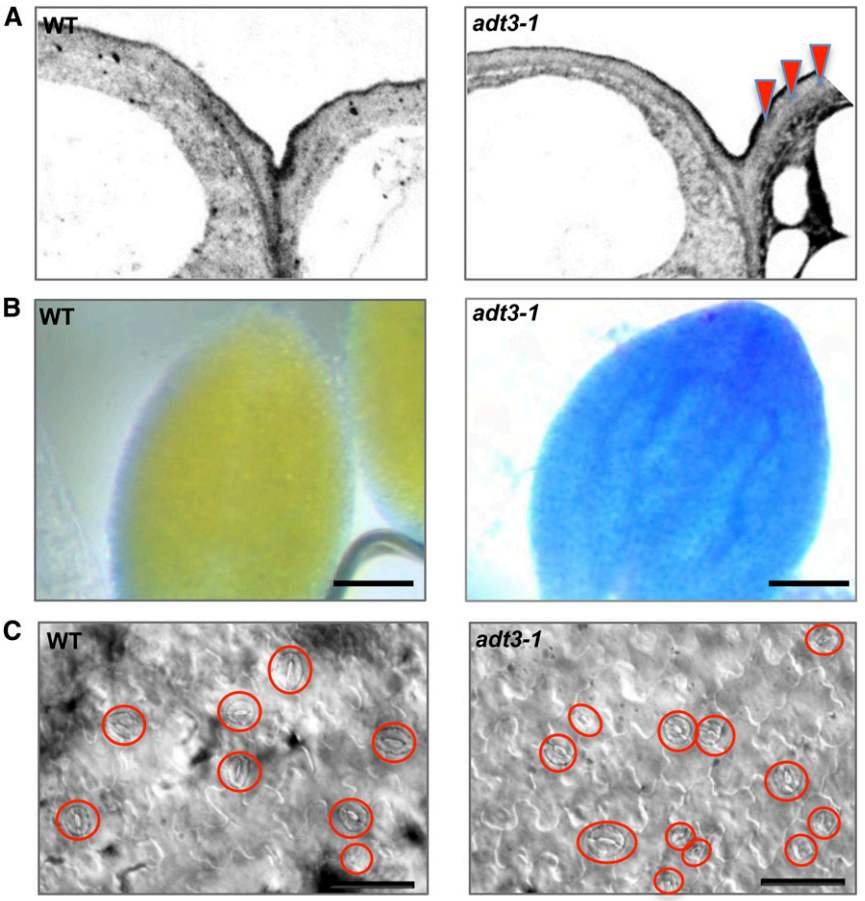

Figure 5. Defective cuticle formation, altered permeability, and aberrant patterning of guard cells in *adt3-1* seedlings. A, Ultrastructure of the cuticle of *adt3-1* epidermis. TEM micrographs of wild-type (WT; top) and *adt3-1* (bottom) epidermis show the deposition of electron-opaque material within the *adt3-1* cell wall (red triangles). B, Increased permeability of *adt3-1* epidermis under hyposmotic treatment. TB penetration is shown in dark-grown, 6-d-old wild-type (top) and *adt3-1* (bottom) seedlings after 48 h of incubation in sterile water. Bars = 50 μm. C, Light-grown (16 h light:8 h dark), 6-d-old *adt3-1* seedlings exhibit abnormal stomatal development; guard cells in the focal plane are circled. Bars = 25 μm.

DISCUSSION

ADT3 Accumulates in the Cytosol and Is Required to Maintain ROS Homeostasis

We reported previously that an arogenate dehydratase activity could be detected in the cytosol of dark-grown young seedlings upon blue light irradiation. In this study, we used transgenic lines expressing CFP-tagged ADT3 to further investigate in vivo ADT3 localization in 4-d-old dark-grown seedlings. Here, ADT3 expression was detected in the shoot, including cotyledons and the SAM (Fig. 1; Supplemental Fig. S2). We also examined the subcellular localization of ADT3 and confirmed that the enzyme accumulates mainly in the cytosol at this stage of seedling development (Fig. 1). This observation adds to the growing body of evidence supporting the existence of extraplastidial pathways for Phe biosynthesis (Yoo et al., 2013). Phe production in the cytosol has important implications, since cytosolic Phe could be channeled directly into secondary metabolism, as the enzymes of the pathways that utilize Phe as a precursor are found outside the plastids. In particular, cytosolic synthesis of Phe would ensure the timely production of antioxidants and photoprotective molecules, which are required to contain the damage caused by high-frequency radiation when etiolated seedlings are exposed to solar light. Accordingly, we reported previously an overall reduction in UV light- and blue light-absorbing compounds in the cotyledon when Phe supply is compromised by the loss of ADT3 (Warpeha et al., 2006). In addition to providing protection from photodamage, we show here that Phe metabolism could counteract the increase in ROS concentration as part of the stress response to high-frequency radiation (Fig. 2; A-H-Mackerness et al., 2001; Kalbina and Strid, 2006; Consentino et al., 2015).

However, ROS levels were elevated significantly in unirradiated *adt3* cotyledon cells compared with wild-type cells (Fig. 2; Supplemental Figs. S3–S5), indicating that ADT3 activity is required to maintain a low basal level of ROS in etiolated seedlings. Because of the high number of mitochondria in the *adt3* mutant cells and the decrease in oil bodies (Fig. 4), we suggest that ROS overproduction could be due to a combination of normal reoxygenation of the germinating tissues when the embryo emerges from the seed coat (Sattler et al., 2004) and the intense metabolic activity that is likely required for the catabolism of the oil bodies.

Increased sensitivity to light and oxidative stress has been reported previously for a mutant of the ROS-scavenging enzyme ASCORBATE PEROXIDASE1

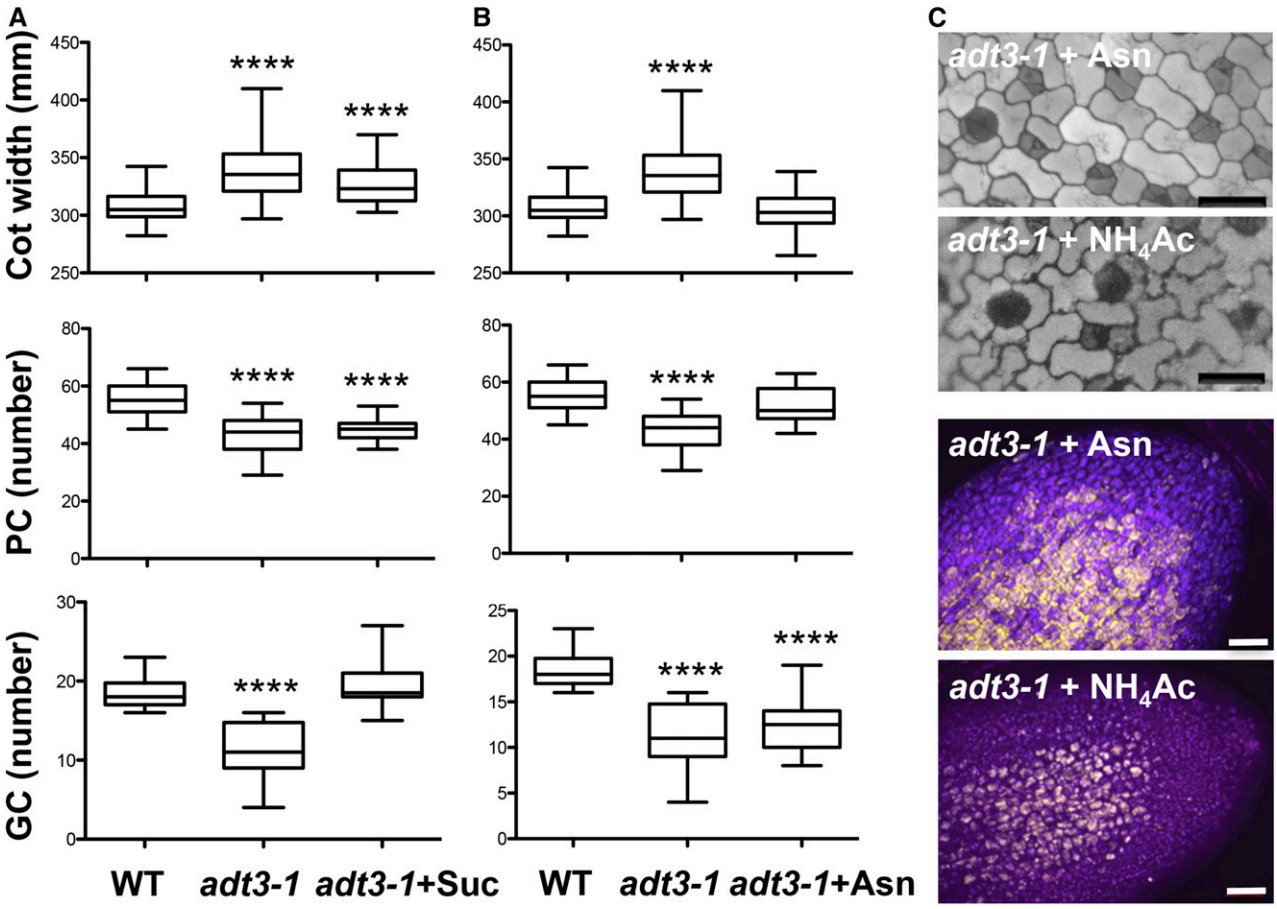

Figure 6. Effects of exogenous Suc, Asn, and NH_3Ac supply on *adt3-1* epidermis. A, Guard cell (GC) number phenotype is rescued by Suc, but not cotyledon (Cot) width or pavement cell (PC) defects of *adt3-1* seedlings. Four-day-old dark-grown seedlings were transferred to 1% Suc, and epidermal phenotypes were quantified 48 h later (6-d-old seedlings). $n = 20$ to 25. ****, $P < 0.0001$. B, Asn supply rescues cotyledon width and pavement cell number phenotypes but not the guard cell lineage in *adt3* seedlings. L-Asn was included in the top agarose at planting. Epidermal phenotypes were measured on day 6. $n = 20$ to 25. ****, $P < 0.0001$. WT, Wild type. C, Asn and NH_3Ac supply restores cotyledon morphology and oil bodies in *adt3* cotyledons. DAPI contrast images (top; bars = 25 μm) and Nile Red signal (bottom; bars = 50 μm) of 6-d-old, dark-grown *adt3* seedlings are shown. Nile Red signal was false-colored gold. Merge of DAPI (blue), FITC (gold), and Cy5 (pink) is shown.

(APX1) gene, which exhibited a low cytosolic content of the antioxidant ascorbic acid (Davletova et al., 2005; Miller et al., 2007). Similar to *apx1*, the *adt3* mutant phenotype could be a consequence of high steady-state cytosolic ROS levels. In Arabidopsis, it has been shown that cytosolic scavenging enzymes are induced upon light stress (Karpinski et al., 1997, 1999; Pnueli et al., 2003; Davletova et al., 2005), even though ROS are thought to be generated in chloroplasts and/or peroxisomes (Mittler, 2002). In addition, buffering ROS in the cytosol was shown to be essential to protect the chloroplast from oxidative damage (Davletova et al., 2005). Indeed, these chemical species can damage the membranes of organelles (Gill and Tuteja, 2010), in particular, plastids (Asada, 2000). Since we observed localization of ADT3 in the cytosol of the cells in etiolated seedlings (Fig. 1), we concluded that cytosolic Phe-derived antioxidants, and even cytosolic Phe per se, may be required to protect the integrity of the plastids from the cytosolic side, a notion that is supported by the abnormal structure of these organelles in *adt3* plastids (Fig. 4), and to preserve their functionality, as indicated by the down-regulation of essential processes that take place in these organelles, such as nitrogen metabolism and the response to oxidative stress (Table I). Indeed, when we irradiated dark-grown wild-type seedlings with high-energy UV-B light (300 nm), we noticed that the structure of the plastids was visibly affected by the treatment and that inclusion of Phe to the growth medium at sowing restored the characteristic prolamellar body organization that was observed before irradiation (Supplemental Fig. S9). The effect was even more dramatic in the *adt3-1* mutant, where plastids were hardly discernible upon UV-B irradiation but were resistant to the treatment in the presence of Phe (Supplemental Fig. S9). This is consistent with the

ability of phenylpropanoids such as flavonols to bind to nonbilayer lipids such as monogalactosyl diacylglycerol (Erlejman et al., 2004). Part of the acute sensitivity of *adt3* seedlings to UV-C irradiation doses that are tolerated by the wild type (Warpeha et al., 2008) also could be explained by the observation that other enzymes involved in ROS removal are down-regulated in *adt3* (Table I; Supplemental Table S1). This could lead to a chronic imbalance between the production of ROS upon high-energy UV light treatment and the ROS-buffering capacity of *adt3* seedlings. Failure to activate additional ROS-scavenging pathways as part of the physiological response to increases in ROS concentration (Sharma et al., 2012) suggests that, without the contribution of ADT3 function, ROS would accumulate above the threshold toxic levels in young etiolated seedlings, resulting in irreversible cellular damage (Sharma et al., 2012).

Thus, Phe biosynthesis through ADT3 activity is required to protect the cotyledons of etiolated seedlings from the deleterious effects of ROS by maintaining a low concentration of these toxic compounds at steady state and by buffering ROS increase as a consequence of photostress. Control of ROS homeostasis is still poorly understood, and advancing the knowledge of Phe and related metabolism will help elucidate the cellular signaling and metabolic processes involved in this important mechanism (Geigenberger and Fernie, 2014).

A Role for ADT3-Supplied Phe in Morphogenesis and Cell Proliferation through Cuticle Assembly

ADT3 was shown previously to participate in the production of epicuticular waxes (Warpeha et al., 2008). In this study, we have shown that the *adt3* epidermis bears signs of alterations in the deposition process (Fig. 5A). This is likely to cause a severe alteration in the rheological properties of *adt3* epidermal cells, particularly when the permeability of *adt3* seedlings is challenged (Fig. 5B). Increased levels of known factors involved in cuticle production and transport indicate that the molecular machineries that act in this process are in place in the *adt3* epidermis (Table I), so the defect might be due to a shortage of substrates (like VLCFAs) or impairment in cuticle assembly. Both hypotheses are plausible, as the VLCFAs are produced by plastids (Yeats and Rose, 2013), whose structure and function appear to be altered in *adt3* (Fig. 4; Table I), or could derive from the degradation of triacylglycerols stored in oil bodies, which are nearly absent in *adt3* mutants (Fig. 4; Supplemental Fig. S6). The presence of osmiophilic compounds in the cytoplasm of *adt3* epidermis suggests that a high amount of lipid substrates is available for the formation of cuticle monomers (Fig. 4B), but the observation that the deposition of electron-opaque material occurs within the deeper layers of the cell wall is a sign that the process is disrupted (Fig. 5A). A similar phenotype was seen previously in the *bodyguard* (*bdg*) mutant, a putative α/β-hydrolase, which is thought to function in cutin biosynthesis or as a cross-linking enzyme (Kurdyukov et al., 2006). Similarly, Phe-derived phenolic components of cutin and cuticular waxes (Nawrath et al., 2013) could participate in cuticle assembly as a cross-linker by reacting with cutin monomers (Pollard et al., 2008). The involvement of phenylpropanoids in cuticle formation has been reported previously for *transparent testa* mutants like *ttg1*, which are regulators of the phenylpropanoid biosynthetic pathway (Koornneef, 1990; Xia et al., 2010), strengthening the hypothesis that decreased Phe availability is linked to the *adt3* defect in cuticle formation. TTG1 also is involved in epidermal development, as it participates in trichome and stomata patterning (Bean et al., 2002). Interestingly, mutations in other genes involved in cuticle formation and up-regulated in the *adt3* mutant, like *FIDDLEHEAD*, also affect the number of trichomes (Yephremov et al., 1999; Wellesen et al., 2001), while different genes involved in the same process, like CER1 and CER6, affect stomatal number (Bird and Gray, 2003).

Thus, Phe-derived compounds (and, hence, ADT3 function) could play a role in cell differentiation by modulating cuticle assembly. Indeed, phenylpropanoids appear to be more abundant in the cuticle of the guard cells, where the natural blue fluorescence that they emit under UV light is higher than in the pavement cells because of either the thickness or the richness of wax-bound phenolics in the epicuticular waxes of the guard cells (Karabourniotis et al., 2001). Cuticle composition influences diffusion rates (Kerstiens, 1996; Schreiber and Riederer, 1996), so tightening of the cuticular structure could confine the effect of developmental cues within the stomatal cell lineage (Guseman et al., 2010; Engineer et al., 2014), while a loose cuticle could facilitate exchanges of signaling molecules to prevent pavement cells from acquiring stomatal identity at later stages of stomatal development. Change of permeability due to a decrease in cell wall resistance could then cause the arrest of stomatal development at the meristemoid stages in *adt3*, with a consequent reduction in the number of stomata, or even at an earlier stage, when the initial precursor stomatal lineage, the mother cells, first differentiate from the protoderm. This would explain not only the reduced number of stomata in *adt3* cotyledons but also the decreased number of pavement cells, as the mother cell divides asymmetrically to generate one pavement cell and one meristemoid (Pillitteri and Torii, 2012). The defective cuticle also could contribute to the enlargement observed for *adt3* pavement cells, as they are incapable of maintaining a correct water balance (Fig. 4B). Interestingly, enlarged pavement cells also are observed in the stomata development mutants *speechless* and *mute* (Tanaka et al., 2013), suggesting that communication signals from the stomata cell lineage can influence the morphology of proximal pavement cells. Hence, our work provides evidence that ADT3 function is

required during early stages of seedling establishment to regulate the development of the epidermal layer by controlling the size of pavement cells and stomatal cell fate acquisition though the modulation of cuticle formation. Further analysis is required to establish the chemical composition of the cuticle at this stage of cotyledon development.

Phe Role in Nutrient Availability

Our finding that loss of ADT3 compromises ROS homeostasis and alters cuticle formation indicates that ADT3 function is required to coordinate defense and development in the seed-to-seedling transition. Moreover, we speculate that Phe synthesis by ADT3 could be implicated in energy production during early stages of plant growth. We have shown that supply of Phe restores lipid synthesis in oil body-depleted *adt3* cotyledons (Fig. 3B; Supplemental Fig. S6). As fatty acid biosynthesis takes place in chloroplasts (Yeats and Rose, 2013), which are severely affected by the loss of ADT3, Phe treatment of *adt3* seedlings could support this process by shielding the developing plastid membranes from the damage caused by increased ROS levels at steady state, therefore preserving their functionality. Alternatively, de novo synthesis of fatty acids could be carried out using Phe as a substrate of the tricarboxylic acid cycle through Tyr conversion; however, resupplying the *adt3* mutant with Tyr did not rescue *adt3* phenotypes (Supplemental Fig. S7). Although we cannot exclude that this may be due to the inability of *adt3* to take up or metabolize Tyr in the form we supplied, it is tempting to speculate that Phe could be metabolized by a pathway that does not encompass the Tyr conversion step (Wang et al., 2013).

We also could rescue fatty acid biosynthesis by supplying the *adt3-1* mutant with Asn and NH_4Ac (Fig. 5), which also led to the restoration of the pavement cell phenotype (Fig. 5). Curiously, the pavement cell defect could not be ameliorated by the addition of Suc, which was instead successful in rescuing the guard cell phenotype in *adt3* cotyledons. Asn is known to be an important nitrogen carrier for transport and storage, and an increase in Asn through up-regulation of ASN1 in dark-grown seedling was shown to be part of a metabolic strategy for the remobilization of metabolites in low-energy states (Lam et al., 1998, 2003). This seems to be the case for XANTHINE DEHYDROGENASE1, whose activity provides a source of nitrogen through purine catabolism (Brychkova et al., 2008). As both proteins are significantly up-regulated in the *adt3* proteome (Supplemental Table S1), we put forward that Phe metabolism may provide an alternative source of nitrogen in etiolated seedlings. Indeed, deamination by Phe ammonia lyase is the first step of Phe metabolism, and the ammonia is thought to be recycled back into Phe biosynthesis (Singh et al., 1998; Corea et al., 2012); however, under nitrogen shortage, Glu from Phe metabolism could be used as an alternative nitrogen source (Lee et al., 2007) or as a nitrogen donor for other pathways, as observed for other organisms (Marusich et al., 1981; Sikora and Marzluf, 1982; Vuralhan et al., 2003). The nitrogen requirement in *adt3* seedlings could be needed to restore an imbalance in carbon-nitrogen ratio that is caused by an increase in carbon availability as a result of cell wall metabolism, as suggested by the up-regulation of SUGAR TRANSPORTER PROTEIN1 and the enrichment in enzymes involved in cell wall remodeling (Table I; Supplemental Table S1; Stadler et al., 2003; Baena-González et al., 2007; Schofield et al., 2009).

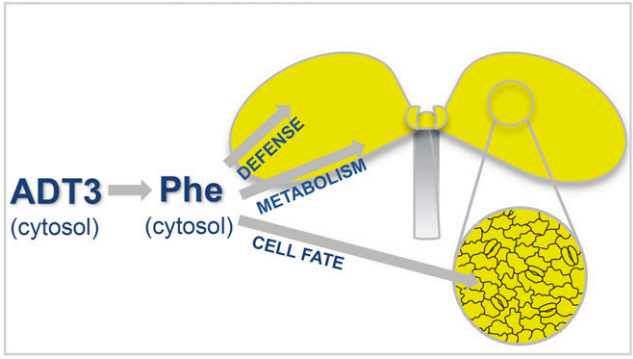

Figure 7. Model indicating multiple potential roles of Phe, mainly produced in the cytosol by ADT3 in Arabidopsis cotyledons at the seed-to-seedling transition.

ADT3 in Signaling and Development

In Arabidopsis, α, β-, and γ-subunits of G-proteins and their effectors are part of complex signal transduction pathways that regulate defense mechanisms and developmental processes (Huang et al., 2006; Pandey et al., 2006; Lee et al., 2013; Urano et al., 2013; Urano and Jones, 2014). G-protein signaling is thought to participate in the developmental program underlying the seed-to-seedling transition by influencing the structure of the cotyledons. Mutations in GPA1, the sole Gα-subunit found to date in Arabidopsis, result in low stomatal density and in an increase in the size of epidermal cells in young seedlings (Ullah et al., 2001; Zhang et al., 2008; Nilson and Assmann, 2010). These observations indicate a defect in cell division and elongation as the possible cause of *gpa1* morphological phenotypes, which also could explain the short hypocotyl and open apical hook of *gpa1* etiolated seedlings (Lease et al., 2001; Ullah et al., 2002, 2003). Interestingly, the assembly of a G-protein interactome has revealed that GPA1 interacts with proteins that are involved in the modulation of cell wall composition or structure (Klopffleisch et al., 2011), like those we reported misregulated in the *adt3* proteome (Table I), providing a possible link between G-proteins and morphogenesis. ADT3 is part of a signaling module that includes GPA1 and GCR1, whose activation by blue light leads to Phe

synthesis (Warpeha et al., 2006, 2008). *gpa1* and *gcr1* mutants are deficient in the production of Phe-derived compounds and share a high degree of phenotypic similarity with *adt3*, including reduced number of stomata, broader cotyledons, and poorly developed chloroplasts (Ullah et al., 2001; Zhang et al., 2008; Nilson and Assmann, 2010), which can be rescued by supplying exogenous Phe (Fig. 3; Supplemental Fig. S10). Therefore, we conclude that ADT3-derived Phe could function as a liaison between signaling and development at the early stages of seed establishment.

CONCLUSION

In this study, we propose a simple model for ADT3 action and the subsequent Phe produced (Fig. 7, inset epidermis). We show that ADT3 localizes mainly in the cytosol of cotyledon cells at the transition from seed to seedling, therefore placing Phe biosynthesis outside the plastid. The existence of an extraplastidic pathway for Phe biosynthesis was speculated previously in Arabidopsis (d'Amato et al., 1984; Benesova and Bode, 1992; Eberhard et al., 1996), and evidence of a cytosolic route for Phe production was reported recently in petunia (*Petunia hybrida*; Yoo et al., 2013). Later in development, ADT3 appears to be localized in the chloroplast of green tissues, suggesting that ADT3 localization appears to be age and light dependent; further investigation will be required to unravel the molecular dynamics of ADT3 function.

Our work opens a window into an elusive phase of plant life, when the seedling has emerged from the seed coat but is not yet capable of carrying on photosynthesis. We demonstrated that cytosolic Phe plays a critical role during the transition from heterotrophy to autotrophy by protecting the cells from oxidative damage, providing substrates for defense, and, possibly, fueling energy pathways. In laboratory conditions, this transition is quite fast, since germination is routinely achieved by planting seeds on synthetic medium in light conditions; however, in natural environments, variables such as light limitation due to dense vegetation could extend the transition, as could the agricultural practice of burying seeds deeper than natural dispersal, making the accumulation of cytosolic Phe critical for survival. Recently, a molecular switch that regulates the allocation of resources to growth and defense was described in which the increase in uncharged $tRNA^{Phe}$ accumulation, as a consequence of the imbalance in Phe metabolism that accompanies pathogen challenge, switches off primary growth and development by repressing the expression of chloroplast proteins and switches on the cellular program that leads to systemic acquired resistance (Pajerowska-Mukhtar et al., 2012). Through a similar mechanism, Phe availability could play a critical role in etiolated seedlings by providing a physical, metabolic, and defense support to the emerging embryo.

MATERIALS AND METHODS

Chemicals

All chemicals, unless noted otherwise, were obtained from Sigma.

Plant Materials, Seed Stocks, and Accessions

Seeds of wild-type Columbia Arabidopsis (*Arabidopsis thaliana*) and T-DNA insertion lines for *ADT3* (At2g27820) *adt3-1* (SALK_029949), and *adt3-6* (SALK_071907) were obtained from the Arabidopsis Biological Resource Center (Alonso et al., 2003). The double mutant (accession no. CS8602) of FAH1-7 (At4g36220; Landry et al., 1995) and TT4-1 (At5g13930; Li et al., 1993) was a gift from Wendy Peer (University of Maryland). The mutant lines are homozygous null for the reported insertions. The mutant *speechless* (At5g53210) was a gift from Keiko Torii (University of Washington); *mute* (At3g06120) was a gift from Dominique Bergmann (Stanford University).

Plant Growth Conditions for Experiments

Seeds of Arabidopsis wild type or T-DNA insertion mutants were sown on 0.5× Murashige and Skoog (MS) medium with no added sugars, hormones, vitamins, or other nutrients in complete darkness using a dim green safelight to prevent photomorphogenesis (Mandoli and Briggs, 1982; Orozco-Nunnelly et al., 2014). For some experiments, seeds were sown on top agarose supplemented with chemicals (500 μM NH_4Ac, 500 μM L-Phe, 500 μM L-Tyr, and 500 μM L-Trp or L-Asn) and then grown for 6 d. For other experiments, 4-d postsowing on 0.5× MS top agarose, disks bearing about 30 seedlings were moved to filter paper soaked with 0.5× MS medium (control), 1% Suc, or 1% mannitol (final concentration in 0.5× MS medium) and then analyzed after 48 h. For most replicates, $n = 30$ unless specified otherwise.

Contrast Microscopy: Deconvoluting

Living seedlings were mounted in sterile water to be viewed on a Zeiss Observer.Z1 deconvoluting microscope utilizing the 20× or 63× (oil-immersion) objective with DAPI excitation to view traditional fluorescence or on an optical apotome utilizing XCite 120 LED/Lumen Dynamics DAPI, FITC, and Cy5 LEDs, as managed by Zen pro software. Images were captured on a high-resolution Axio503 mono camera. At least 30 seedlings were viewed per experimental condition for experiments unless described otherwise (20–40 seedlings per experimental condition for analysis). A 150-μm square superimposed on images was analyzed to quantitate cell type numbers, and cell area was quantified using Image J (http://imagej.nih.gov/ij/).

Cellular Stress Assays

Four days after moving to 20°C, dark-grown seedlings were placed on sterile filter paper for 3 h with 0.5× MS medium (control), potassium iodide, Phe, or the analog *para*-DL-fluoro-Phe (Conway et al., 1963). Seedlings received an empircally determined sublethal (3-min) dose of 254 nm (UV light methods are described in Warpeha et al., 2008). Young cotyledons emit natural fluorescence after absorption of UV (DAPI; Warpeha et al., 2008) or blue/blue-green (FITC; Tattini et al., 2004; Warpeha et al., 2008) irradiation, so these LEDs were used to collect fluorescence information. The specific cell-permeable dye CellRox Deep Red (Life Technologies) emitting in the red/far-red region was used as recommended by the manufacturer to detect ROS dark-grown seedlings (Cy5 channel, false-colored pink; Ghura et al., 2016). In brief, dark-grown seedlings of the wild type or *adt3* (each replicate had 30 seedlings) on day 6 were exposed to a sublethal treatment of UV-C light (254 nm), then cut mid hypocotyl to be immediately immersed in 400 μL of 5 μM CellRox in sterile dimethyl sulfoxide in a glass well dish in darkness. Samples were orbitally rotated (50 rpm) for 30 min. At that time, CellRox reagent was removed by a p200 pipet tip to avoid removing cut seedlings, then solution was replaced immediately by sterile 1× phosphate-buffered saline (PBS; pH 7.2) for three 3-min washes under the same rotation. After washing, the PBS was removed and seedlings were rinsed one time in sterile water for 3 min and then mounted in sterile water on glass slides for immediate microscopy. Cotyledons were imaged with 63× (oil-immersion) and, for some experiments, 20× objectives with DAPI, FITC, and Cy5 LEDs in 1-μm optical sections by apotome (microscope described above). At least 20 seedlings were viewed per replicate, and all exposure settings were based on

the wild-type untreated cotyledons (that setting was used for all seedling conditions and genotypes). For seedlings exposed to Phe, seedlings were moved on day 6 to 500 μM L-Phe for 3 h and then subjected to the same conditions for CellRox reagent experiments. All growth conditions and seedling manipulations were identical for SOSG (Thermo Fisher); however, the preparations of the reagent were as follows. SOSG is provided as a solid and was dissolved as directed in methanol to 5 mM. The working solution was utilized at 10 μM in 1× PBS (pH 7.2). Identically to CellRox experiments, seedlings were immersed in the reagent immediately postirradiation, then washed in the same way, and mounted in sterile water for microscopy. Microscopy was handled in the same way as for CellRox reagent, except that SOSG responds to singlet oxygen by causing a large fluorescence that can be captured by FITC. The LEDs utilized for these experiments were DAPI, FITC, and Texas Red. As for CellRox, the wild-type unirradiated sample was the replicate used to determine the best exposure, and all other samples used the identical exposure settings. For all fluorescence experiments, epidermal pavement cells were traced in ImageJ, and the fluorescence level (artificial units) was determined and then compared (Ghura et al., 2016). A minimum of six cells per cotyledon of four to six seedlings per replicate were assessed utilizing Prism (see "Statistics").

Nile Red Staining

Six-day-old dark-grown seedlings were cut into 1 mM Nile Red stain (saturated solution in acetone as directed by the manufacturer [Sigma]; working solution in 1× PBS, pH 7.2, was made immediately before use and maintained in darkness throughout) and incubated for 30 min under rotation, with the same experimental handling and timing as SOSG. Seedlings then were mounted in sterile water as described for SOSG and visualized by optical sectioning (described above) at 20× magnification using FITC (false-colored gold). $n = 30$ for each replicate.

Cloning

Standard molecular biology techniques and the Gateway system (Invitrogen) were used for all cloning procedures as described (Orozco-Nunnelly et al., 2014). The 819-bp *ADT3* promoter fragment was cloned into pDONR P4-P1R (Invitrogen), and the *ADT3* open reading frame fragment was cloned into pENTR/D-TOPO (Invitrogen). pGreen (Hellens et al., 2000) was used as the destination vector for the construct *ADT3*::ADT3-GFP or *ADT3*::ADT3-CFP. T3 homozygous transformed seedlings were used in experiments.

Visualization of Transgene Expression by Spinning Disk Confocal Microscopy

Transgenic and untransformed 4-d-old dark-grown seedlings were mounted live and immediately viewed on an Andor WD Spinning Disk confocal system using iQ3 software as described (Orozco-Nunnelly et al., 2014). LEDs at 1 nm width included 405 nm (DAPI; blue), 488 nm (GFP; green), 445 nm (CFP; magenta), and 561 nm (red). Images were captured at 30× or 60× as described, with 1-μm optical section thickness. Images were prepared with ImageJ software. $n = 20$ for each replicate.

TEM

Seedlings were harvested into 0.5× Karnovsky's fixative for overnight storage at 4°C, and buffer was washed and then fixed in 1% OSO_4 for 2 h. After washes in 0.1 M cacodylate buffer, the samples were embedded in 3% SeaPrep agar, dehydrated in a 10% to 100% ethanol series, and infiltrated with Spurr's resin, which was allowed to polymerize at 70°C for 2 d. Thin sections (between 70 and 80 nm) of at least five seedlings for each sample were cut on a Leica UC7 ultramicrotome, collected on a 200-mesh formvar/carbon-coated copper grid (Ted Pella), and stained with aqueous UA for 2 h and lead citrate for 5 min. The grids were viewed with a JEOL JEM 1400 TEM device, and images were taken at 120 kV.

TB Staining

On day 4, dark-grown seedling islands of top agarose were transplanted to 0.5× MS medium in phytatrays with disk annealed by a 200-μL top agarose drop to the tray. The bottom of the phytatray was covered with sterile water only or 0.5× MS medium, and on day 6, the phytatray was filled with TB solution to cover the seedlings (Tanaka et al., 2004). After 3 min, seedlings were washed and immediately imaged with a bright-field Zeiss V.2 stereo dissecting microscope.

Statistics

Data shown in the figures were entered into Prism version 5.0 (GraphPad Software; graphpad.com), where means and SE were calculated for relevant experiments. Unpaired Student's t test with Welch's correction was used to assess significance.

Protein Extraction, Digestion, Labeling, and Subfractionation

Protein was extracted from each biological replicate of 6-d-old dark-grown wild-type and *adt3* liquid nitrogen-ground samples as described previously (Alvarez et al., 2011). The pellets were then dissolved in 150 μL of 3 M urea and 0.5 M triethylammonium bicarbonate, pH 8.5, and assayed using the CB-X protein assay kit (G-Biosciences). Each sample was reduced in a final concentration of 5 mM Tris-(2-carboxyethyl)-phosphine hydrochloride for 1 h at 37°C and alkylated using 10 mM iodoacetamide for 30 min at 22°C in the dark. Aliquots containing 40 μg of protein were diluted to 1 M urea and digested with trypsin at a 1:20 enzyme:protein ratio for 16 h at 37°C. Samples were desalted using 1-mL Sep-Pak Vac C18 solid-phase extraction columns (Waters) and vacuum centrifuged (Centrivap; Labconco) to dryness. Stable isotope labeling was carried out with TMT-6plex reagents (Thermo Fisher Scientific) according to the manufacturer's instructions, and the six samples were combined, vacuum centrifuged, and desalted using solid-phase extraction. Subfractionation was carried out on a 3100 OFFGEL fractionator (Agilent Technologies) using pH 3 to 10 gradient strips and ampholytes according to the manufacturer's guidelines, but without the incorporation of glycerol. Focusing was carried out for 50 kilowatt hours with a current limit of 50 μA and a voltage limit of 8,000 V. Fractions were fully dried.

Protein Identification and Quantification by Liquid Chromatography-Tandem Mass Spectrometry

Liquid chromatography-tandem mass spectrometry was carried out on a LTQ-Orbitrap Velos Pro (Thermo Fisher Scientific) as described previously (Alvarez et al., 2013, 2014) coupled with a U3000 RSLCnano HPLC device (Thermo Fisher Scientific). The dried OFFGEL fractions were dissolved in 5% acetonitrile and 0.1% formic acid, and a portion was loaded onto a C_{18} trap column (PepMap100; 300-μm i.d. × 5 mm, 5-μm particle size, 100 Å; Thermo Fisher Scientific) at a flow rate of 15 μL min^{-1} for 4 min equilibrated with 2% acetonitrile and 0.1% formic acid. Peptide separation was carried out on a C_{18} column (Acclaim PepMap RSLC; 15 cm × 75 μm nanoViper, C18, 2 μm, 100 Å; Thermo Fisher Scientific) at a flow rate of 0.3 μL min^{-1} and the following gradient: 0 to 3 min, 2% B isocratic; 3 to 12 min, 2% to 15% B; 12 to 84 min, 15% to 38% B; 84 to 93 min, 38% to 50% B; and 93 to 97 min, 50% to 90% B. Mobile phase A was 0.1% formic acid, and mobile phase B was 0.1% formic acid in 80:20 acetonitrile:water. The Orbitrap mass analyzer was operated as described previously (Alvarez et al., 2014), except for the exclusion duration, which was set at 90 s, and the minimum mass spectrometry ion count for triggering tandem mass spectrometry, which was set to 50,000 counts.

Database Search and Data Mining for the Proteome

Data processing was automated using Mascot Daemon (Matrix Science). Mascot Distiller, version 2.4.3.3 64 bit (Matrix Science), was used to create mgf files, which Mascot Server, version 2.4 (Matrix Science), searched against The Arabidopsis Information Resource 10 (35,386 entries) to identify and quantify the proteins with a false discovery rate of 1%. The search parameters used have been described previously (Alvarez et al., 2014) except for the fixed modifications, which were set as TMT (N-terminal) and TMT (K). Only proteins with at least two peptides were used for the analysis. Peptide and protein ratios were calculated using the weighted method in Mascot, where the intensity values of the set of peptides are summed and the protein ratios are calculated from the summed values. Normalization of the ratios was performed using the total labeling intensity of each species (summed intensities). The ratios and SD values for all combinations of the replicates *adt3*/wild type were

reported. An overall ratio for a protein hit was reported only if the minimum number of two peptide matches was achieved. If the ratios for the peptide matches were not consistent with a sample from a normal distribution, the ratios were not used further in the analysis. Only protein ratios statistically different from 1 ($P < 0.05$), detected from the replicates, were averaged. Only proteins for which there were at least three protein ratios, of which at least one was associated with each control for each of the three mutant replicates, were used for further analyses. For these proteins, the SD and coefficient of variation were calculated.

The proteome was analyzed using the bioinformatics platform Virtual Plant (http://virtualplant.bio.nyu.edu/cgi-bin/vpweb/; Katari et al., 2010) and the KEGG database (http://www.genome.jp/kegg/).

Supplemental Data

The following supplemental materials are available.

Supplemental Figure S1. *ADT3*::ADT3-GFP restores *adt3-1* cotyledon epidermis to wild-type appearance and confers survival to UV light stress.

Supplemental Figure S2. Expression of ADT3-GFP fusions in *adt3-1* and wild-type backgrounds and *ADT3*::ADT3-GFP in the SAM.

Supplemental Figure S3. ROS detection in the *adt3-6* mutant by CellRox.

Supplemental Figure S4. Singlet oxygen species detection in *adt3* mutant seedlings incubated with SOSG.

Supplemental Figure S5. ROS levels detected by CellRox from unirradiated and UV-C irradiated wild-type and *adt3-1* seedling cotyledons before and after pretreatment with Phe, the ROS scavenger potassium iodide, and a Phe analog.

Supplemental Figure S6. Epidermal defects in *adt3-6* seedlings are rescued by Phe.

Supplemental Figure S7. Phenotypic defects of *adt3-1* seedlings not complemented by Tyr or Trp; stomatal lineage mutants do not respond to Phe like *adt3-1* mutants.

Supplemental Figure S8. Experiments indicate that mannitol does not rescue guard cell lineage progression.

Supplemental Figure S9. Developing chloroplast ultrastructural phenotype rescue in *adt3* mesophyll cells by inclusion of Phe in planting medium,

Supplemental Figure S10. *gpa1* and *gcr1* mutants have cotyledon phenotypes that can be rescued by Phe.

Supplemental Table S1. Proteome data of 6-d dark-grown *adt3-1* mutant compared with the wild type.

Supplemental Table S2. PO analysis for up-regulated proteins in the *adt3* proteome.

Supplemental Table S3. GO term analysis for biological process for *adt3* up-regulated proteins in the epidermal cell PO category.

Supplemental Table S4. GO term analysis for cell components for up-regulated proteins in the *adt3* proteome.

Supplemental Table S5. GO term analysis for biological process for *adt3* up-regulated proteins in the plasma membrane category.

Supplemental Table S6. GO term analysis for biological process for *adt3* up-regulated proteins in the vacuole category.

Supplemental Table S7. GO term analysis for biological process for *adt3* up-regulated proteins in the cell wall category.

Supplemental Table S8. PO analysis for down-regulated proteins in the *adt3* proteome.

Supplemental Table S9. GO term analysis for molecular function for *adt3* down-regulated proteins in the epidermal cell PO category.

Supplemental Table S10. GO term analysis for cell components for down-regulated proteins in the *adt3* proteome.

Supplemental Table S11. GO term analysis for biological process for down-regulated proteins in the *adt3* proteome.

ACKNOWLEDGMENTS

We thank Jennifer Baek, Ashley Williams, Yang Chen, Huini Wu, and Nadia Kukuruza for assistance with experiments; Dr. Jeremy Lynch and Dr. Teresa Orenic for assistance with confocal and deconvoluting microscopy, respectively; Jack Gibbons for electron microscopy services featured in the Supplemental Data; Stephen MacFarlane, Sharmon Knecht, and especially Bobbie Schneider for TEM (Fred Hutchinson Cancer Center); John Cason for artwork, except Figure 7; and Dr. Lon Kaufman (now at City University of New York-Hunter College) and Dr. Gary Gardner (University of Minnesota) for helpful discussion.

Received March 30, 2016; accepted August 15, 2016; published August 18, 2016.

LITERATURE CITED

Agati G, Brunetti C, Di Ferdinando M, Ferrini F, Pollastri S, Tattini M (2013) Functional roles of flavonoids in photoprotection: new evidence, lessons from the past. Plant Physiol Biochem **72:** 35–45

A-H-Mackerness S, John CF, Jordan B, Thomas B (2001) Early signaling components in ultraviolet-B responses: distinct roles for different reactive oxygen species and nitric oxide. FEBS Lett **489:** 237–242

Alonso JM, Stepanova AN, Leisse TJ, Kim CJ, Chen H, Shinn P, Stevenson DK, Zimmerman J, Barajas P, Cheuk R, et al (2003) Genome-wide insertional mutagenesis of Arabidopsis thaliana. Science **301:** 653–657

Alvarez S, Hicks LM, Pandey S (2011) ABA-dependent and -independent G-protein signaling in Arabidopsis roots revealed through an iTRAQ proteomics approach. J Proteome Res **10:** 3107–3122

Alvarez S, Roy Choudhury S, Hicks LM, Pandey S (2013) Quantitative proteomics-based analysis supports a significant role of GTG proteins in regulation of ABA response in Arabidopsis roots. J Proteome Res **12:** 1487–1501

Alvarez S, Roy Choudhury S, Pandey S (2014) Comparative quantitative proteomics analysis of the ABA response of roots of drought-sensitive and drought-tolerant wheat varieties identifies proteomic signatures of drought adaptability. J Proteome Res **13:** 1688–1701

Apel K, Hirt H (2004) Reactive oxygen species: metabolism, oxidative stress, and signal transduction. Annu Rev Plant Biol **55:** 373–399

Asada K (2000) The water-water cycle as alternative photon and electron sinks. Philos Trans R Soc Lond B Biol Sci **355:** 1419–1431

Baena-González E, Rolland F, Thevelein JM, Sheen J (2007) A central integrator of transcription networks in plant stress and energy signalling. Nature **448:** 938–942

Bar-Peled M, O'Neill MA (2011) Plant nucleotide sugar formation, interconversion, and salvage by sugar recycling. Annu Rev Plant Biol **62:** 127–155

Bean GJ, Marks MD, Hülskamp M, Clayton M, Croxdale JL (2002) Tissue patterning of Arabidopsis cotyledons. New Phytol **153:** 461–467

Benesova M, Bode R (1992) Chorismate mutase isoforms from seeds and seedlings of Papaver somniferum. Phytochemistry **31:** 2983–2987

Bird SM, Gray JE (2003) Signals from the cuticle affect epidermal cell differentiation. New Phytol **157:** 9–23

Bross CD, Corea OR, Kaldis A, Menassa R, Bernards MA, Kohalmi SE (2011) Complementation of the pha2 yeast mutant suggests functional differences for arogenate dehydratases from Arabidopsis thaliana. Plant Physiol Biochem **49:** 882–890

Brychkova G, Fluhr R, Sagi M (2008) Formation of xanthine and the use of purine metabolites as a nitrogen source in Arabidopsis plants. Plant Signal Behav **3:** 999–1001

Cho MH, Corea OR, Yang H, Bedgar DL, Laskar DD, Anterola AM, Moog-Anterola FA, Hood RL, Kohalmi SE, Bernards MA, et al (2007) Phenylalanine biosynthesis in Arabidopsis thaliana: identification and characterization of arogenate dehydratases. J Biol Chem **282:** 30827–30835

Consentino L, Lambert S, Martino C, Jourdan N, Bouchet PE, Witczak J, Castello P, El-Esawi M, Corbineau F, d'Harlingue A, et al (2015) Blue-light dependent reactive oxygen species formation by Arabidopsis cryptochrome may define a novel evolutionarily conserved signaling mechanism. New Phytol **206:** 1450–1462

Conway TW, Lansford EM Jr, Shive W (1963) Influence of phenylalanine analogues upon bacterial accumulation and incorporation of phenylalanine. J Bacteriol **85:** 141–149

Corea ORA, Bedgar DL, Davin LB, Lewis NG (2012) The arogenate dehydratase gene family: towards understanding differential regulation of carbon flux through phenylalanine into primary versus secondary metabolic pathways. Phytochemistry **82:** 22–37

d'Amato TA, Ganson RJ, Gaines CG, Jensen RA (1984) Subcellular localization of chorismate-mutase isoenzymes in protoplasts from mesophyll and suspension-cultured cells of Nicotiana silvestris. Planta **162:** 104–108

Davletova S, Rizhsky L, Liang H, Shengqiang Z, Oliver DJ, Coutu J, Shulaev V, Schlauch K, Mittler R (2005) Cytosolic ascorbate peroxidase 1 is a central component of the reactive oxygen gene network of *Arabidopsis*. Plant Cell **17:** 268–281

Eberhard J, Ehrler TT, Epple P, Felix G, Raesecke HR, Amrhein N, Schmid J (1996) Cytosolic and plastidic chorismate mutase isozymes from Arabidopsis thaliana: molecular characterization and enzymatic properties. Plant J **10:** 815–821

Engineer CB, Ghassemian M, Anderson JC, Peck SC, Hu H, Schroeder JI (2014) Carbonic anhydrases, EPF2 and a novel protease mediate CO_2 control of stomatal development. Nature **513:** 246–250

Erlejman AG, Verstraeten SV, Fraga CG, Oteiza PI (2004) The interaction of flavonoids with membranes: potential determinant of flavonoid antioxidant effects. Free Radic Res **38:** 1311–1320

Fell D, Cornish-Bowden A (1997) Understanding the Control of Metabolism, **Vol 2**. Portland Press, London

Finch-Savage WE, Leubner-Metzger G (2006) Seed dormancy and the control of germination. New Phytol **171:** 501–523

Geigenberger P, Fernie AR (2014) Metabolic control of redox and redox control of metabolism in plants. Antioxid Redox Signal **21:** 1389–1421

Ghura S, Tai L, Zhao M, Collins N, Che CT, Warpeha KM, LaDu MJ (2016) *Arabidopsis thaliana* extracts optimized for polyphenols production as potential therapeutics for the *APOE*-modulated neuroinflammation characteristic of Alzheimer's disease *in vitro*. Sci Rep **6:** 29364

Gill SS, Tuteja N (2010) Reactive oxygen species and antioxidant machinery in abiotic stress tolerance in crop plants. Plant Physiol Biochem **48:** 909–930

Gray JE, Holroyd GH, van der Lee FM, Bahrami AR, Sijmons PC, Woodward FI, Schuch W, Hetherington AM (2000) The HIC signalling pathway links CO_2 perception to stomatal development. Nature **408:** 713–716

Greenspan P, Mayer EP, Fowler SD (1985) Nile Red: a selective fluorescent stain for intracellular lipid droplets. J Cell Biol **100:** 965–973

Guseman JM, Lee JS, Bogenschutz NL, Peterson KM, Virata RE, Xie B, Kanaoka MM, Hong Z, Torii KU (2010) Dysregulation of cell-to-cell connectivity and stomatal patterning by loss-of-function mutation in Arabidopsis chorus (glucan synthase-like 8). Development **137:** 1731–1741

Hanson MR, Sattarzadeh A (2011) Stromules: recent insights into a long neglected feature of plastid morphology and function. Plant Physiol **155:** 1486–1492

Hellens RP, Edwards EA, Leyland NR, Bean S, Mullineaux PM (2000) pGreen: a versatile and flexible binary Ti vector for Agrobacterium-mediated plant transformation. Plant Mol Biol **42:** 819–832

Holdsworth MJ, Finch-Savage WE, Grappin P, Job D (2008) Post-genomics dissection of seed dormancy and germination. Trends Plant Sci **13:** 7–13

Hruz T, Laule O, Szabo G, Wessendorp F, Bleuler S, Oertle L, Widmayer P, Gruissem W, Zimmermann P (2008) Genevestigator v3: a reference expression database for the meta-analysis of transcriptomes. Adv Bioinformatics **2008:** 420747

Huang J, Taylor JP, Chen JG, Uhrig JF, Schnell DJ, Nakagawa T, Korth KL, Jones AM (2006) The plastid protein THYLAKOID FORMATION1 and the plasma membrane G-protein GPA1 interact in a novel sugar-signaling mechanism in *Arabidopsis*. Plant Cell **18:** 1226–1238

Kacser H, Burns JA (1995) The control of flux. Biochem Soc Trans **23:** 341–366

Kalbina I, Strid A (2006) The role of NADPH oxidase and MAP kinase phosphatase in UV-B-dependent gene expression in Arabidopsis. Plant Cell Environ **29:** 1783–1793

Karabourniotis G, Tzobanoglou D, Nikolopoulos D, Liakopoulos G (2001) Epicuticular phenolics over guard cells: exploitation for in situ stomatal counting by fluorescence microscopy and combined image analysis. Ann Bot (Lond) **87:** 631–639

Karpinski S, Escobar C, Karpinska B, Creissen G, Mullineaux PM (1997) Photosynthetic electron transport regulates the expression of cytosolic ascorbate peroxidase genes in *Arabidopsis* during excess light stress. Plant Cell **9:** 627–640

Karpinski S, Reynolds H, Karpinska B, Wingsle G, Creissen G, Mullineaux P (1999) Systemic signaling and acclimation in response to excess excitation energy in Arabidopsis. Science **284:** 654–657

Katari MS, Nowicki SD, Aceituno FF, Nero D, Kelfer J, Thompson LP, Cabello JM, Davidson RS, Goldberg AP, Shasha DE, et al (2010) VirtualPlant: a software platform to support systems biology research. Plant Physiol **152:** 500–515

Kerstiens G (1996) Signalling across the divide: a wider perspective of cuticular structure-function relationships. Trends Plant Sci **1:** 125–129

Klopffleisch K, Phan N, Augustin K, Bayne RS, Booker KS, Botella JR, Carpita NC, Carr T, Chen JG, Cooke TR, et al (2011) Arabidopsis G-protein interactome reveals connections to cell wall carbohydrates and morphogenesis. Mol Syst Biol **7:** 532

Koornneef M (1990) Mutations affecting the testa colour in Arabidopsis. Arabidopsis Information Service **27:** 1–4

Kunst L, Samuels L (2009) Plant cuticles shine: advances in wax biosynthesis and export. Curr Opin Plant Biol **12:** 721–727

Kurdyukov S, Faust A, Nawrath C, Bär S, Voisin D, Efremova N, Franke R, Schreiber L, Saedler H, Métraux JP, et al (2006) The epidermis-specific extracellular BODYGUARD controls cuticle development and morphogenesis in *Arabidopsis*. Plant Cell **18:** 321–339

Lam HM, Hsieh MH, Coruzzi G (1998) Reciprocal regulation of distinct asparagine synthetase genes by light and metabolites in Arabidopsis thaliana. Plant J **16:** 345–353

Lam HM, Wong P, Chan HK, Yam KM, Chen L, Chow CM, Coruzzi GM (2003) Overexpression of the ASN1 gene enhances nitrogen status in seeds of Arabidopsis. Plant Physiol **132:** 926–935

Landry LG, Chapple CC, Last RL (1995) Arabidopsis mutants lacking phenolic sunscreens exhibit enhanced ultraviolet-B injury and oxidative damage. Plant Physiol **109:** 1159–1166

Lease KA, Wen J, Li J, Doke JT, Liscum E, Walker JC (2001) A mutant *Arabidopsis* heterotrimeric G-protein beta subunit affects leaf, flower, and fruit development. Plant Cell **13:** 2631–2641

Lee S, Rojas CM, Ishiga Y, Pandey S, Mysore KS (2013) Arabidopsis heterotrimeric G-proteins play a critical role in host and nonhost resistance against Pseudomonas syringae pathogens. PLoS ONE **8:** e82445

Lee YH, Foster J, Chen J, Voll LM, Weber APM, Tegeder M (2007) AAP1 transports uncharged amino acids into roots of Arabidopsis. Plant J **50:** 305–319

Li J, Ou-Lee TM, Raba R, Amundson RG, Last RL (1993) *Arabidopsis* flavonoid mutants are hypersensitive to UV-B irradiation. Plant Cell **5:** 171–179

Lü B, Wang J, Zhang Y, Wang H, Liang J, Zhang J (2012) AT14A mediates the cell wall-plasma membrane-cytoskeleton continuum in Arabidopsis thaliana cells. J Exp Bot **63:** 4061–4069

MacAlister CA, Ohashi-Ito K, Bergmann DC (2007) Transcription factor control of asymmetric cell divisions that establish the stomatal lineage. Nature **445:** 537–540

Maeda H, Dudareva N (2012) The shikimate pathway and aromatic amino acid biosynthesis in plants. Annu Rev Plant Biol **63:** 73–105

Mandoli DF, Briggs WR (1982) Optical properties of etiolated plant tissues. Proc Natl Acad Sci USA **79:** 2902–2906

Marusich WC, Jensen RA, Zamir LO (1981) Induction of L-phenylalanine ammonia-lyase during utilization of phenylalanine as a carbon or nitrogen source in Rhodotorula glutinis. J Bacteriol **146:** 1013–1019

Miller G, Suzuki N, Rizhsky L, Hegie A, Koussevitzky S, Mittler R (2007) Double mutants deficient in cytosolic and thylakoid ascorbate peroxidase reveal a complex mode of interaction between reactive oxygen species, plant development, and response to abiotic stresses. Plant Physiol **144:** 1777–1785

Mittler R (2002) Oxidative stress, antioxidants and stress tolerance. Trends Plant Sci **7:** 405–410

Mittler R, Vanderauwera S, Suzuki N, Miller G, Tognetti VB, Vandepoele K, Gollery M, Shulaev V, Van Breusegem F (2011) ROS signaling: the new wave? Trends Plant Sci **16:** 300–309

Nawrath C, Schreiber L, Franke RB, Geldner N, Reina-Pinto JJ, Kunst L (2013) Apoplastic diffusion barriers in Arabidopsis. The Arabidopsis Book **11:** e0167, doi/10.1199/tab.0167

Nilson SE, Assmann SM (2010) The α-subunit of the Arabidopsis heterotrimeric G protein, GPA1, is a regulator of transpiration efficiency. Plant Physiol **152:** 2067–2077

Orozco-Nunnelly DA, Muhammad D, Mezzich R, Lee BS, Jayathilaka L, Kaufman LS, Warpeha KM (2014) Pirin1 (PRN1) is a multifunctional protein that regulates quercetin, and impacts specific light and UV responses in the seed-to-seedling transition of Arabidopsis thaliana. PLoS ONE **9:** e93371

Pajerowska-Mukhtar KM, Wang W, Tada Y, Oka N, Tucker CL, Fonseca JP, Dong X (2012) The HSF-like transcription factor TBF1 is a major molecular switch for plant growth-to-defense transition. Curr Biol **22:** 103–112

Pandey S, Chen JG, Jones AM, Assmann SM (2006) G-protein complex mutants are hypersensitive to abscisic acid regulation of germination and postgermination development. Plant Physiol **141:** 243–256

Peer WA, Brown DE, Tague BW, Muday GK, Taiz L, Murphy AS (2001) Flavonoid accumulation patterns of *transparent testa* mutants of Arabidopsis. Plant Physiol **126:** 536–548

Pillitteri LJ, Sloan DB, Bogenschutz NL, Torii KU (2007) Termination of asymmetric cell division and differentiation of stomata. Nature **445:** 501–505

Pillitteri LJ, Torii KU (2012) Mechanisms of stomatal development. Annu Rev Plant Biol **63:** 591–614

Pnueli L, Liang H, Rozenberg M, Mittler R (2003) Growth suppression, altered stomatal responses, and augmented induction of heat shock proteins in cytosolic ascorbate peroxidase (Apx1)-deficient Arabidopsis plants. Plant J **34:** 187–203

Pollard M, Beisson F, Li Y, Ohlrogge JB (2008) Building lipid barriers: biosynthesis of cutin and suberin. Trends Plant Sci **13:** 236–246

Raven PH, Evert RF, Eichhorn SE (2005) Biology of Plants. Macmillan, New York

Rippert P, Puyaubert J, Grisollet D, Derrier L, Matringe M (2009) Tyrosine and phenylalanine are synthesized within the plastids in Arabidopsis. Plant Physiol **149:** 1251–1260

Rozema J, Björn LO, Bornman JF, Gaberščik A, Häder DP, Trošt T, Germ M, Klisch M, Gröniger A, Sinha RP, et al (2002) The role of UV-B radiation in aquatic and terrestrial ecosystems: an experimental and functional analysis of the evolution of UV-absorbing compounds. J Photochem Photobiol B **66:** 2–12

Sattler SE, Gilliland LU, Magallanes-Lundback M, Pollard M, DellaPenna D (2004) Vitamin E is essential for seed longevity and for preventing lipid peroxidation during germination. Plant Cell **16:** 1419–1432

Schofield RA, Bi YM, Kant S, Rothstein SJ (2009) Over-expression of STP13, a hexose transporter, improves plant growth and nitrogen use in Arabidopsis thaliana seedlings. Plant Cell Environ **32:** 271–285

Schreiber L, Riederer M (1996) Determination of diffusion coefficients of octadecanoic acid in isolated cuticular waxes and their relationship to cuticular water permeabilities. Plant Cell Environ **19:** 1075–1082

Seifert GJ (2004) Nucleotide sugar interconversions and cell wall biosynthesis: how to bring the inside to the outside. Curr Opin Plant Biol **7:** 277–284

Sharma P, Jha AB, Dubey RS, Pessarakli M (2012) Reactive oxygen species, oxidative damage, and antioxidative defense mechanism in plants under stressful conditions. J Bot **2012:** 217037

Sikora LA, Marzluf GA (1982) Regulation of L-phenylalanine ammonia-lyase by L-phenylalanine and nitrogen in Neurospora crassa. J Bacteriol **150:** 1287–1291

Singh S, Lewis NG, Towers GH (1998) Nitrogen recycling during phenylpropanoid metabolism in sweet potato tubers. J Plant Physiol **153:** 316–323

Stadler R, Büttner M, Ache P, Hedrich R, Ivashikina N, Melzer M, Shearson SM, Smith SM, Sauer N (2003) Diurnal and light-regulated expression of AtSTP1 in guard cells of Arabidopsis. Plant Physiol **133:** 528–537

Steyn WJ, Wand SJE, Holcroft DM, Jacobs G (2002) Anthocyanins in vegetative tissues: a proposed unified function in photoprotection. New Phytol **155:** 349–361

Takahashi T, Gasch A, Nishizawa N, Chua NH (1995) The DIMINUTO gene of Arabidopsis is involved in regulating cell elongation. Genes Dev **9:** 97–107

Tanaka T, Tanaka H, Machida C, Watanabe M, Machida Y (2004) A new method for rapid visualization of defects in leaf cuticle reveals five intrinsic patterns of surface defects in Arabidopsis. Plant J **37:** 139–146

Tanaka Y, Nose T, Jikumaru Y, Kamiya Y (2013) ABA inhibits entry into stomatal-lineage development in Arabidopsis leaves. Plant J **74:** 448–457

Tattini M, Galardi C, Pinelli P, Massai R, Remorini D, Agati G (2004) Differential accumulation of flavonoids and hydroxycinnamates in leaves of Ligustrum vulgare under excess light and drought stress. New Phytol **163:** 547–561

Tsukagoshi H, Busch W, Benfey PN (2010) Transcriptional regulation of ROS controls transition from proliferation to differentiation in the root. Cell **143:** 606–616

Tzin V, Galili G (2010) New insights into the shikimate and aromatic amino acids biosynthesis pathways in plants. Mol Plant **3:** 956–972

Ullah H, Chen JG, Temple B, Boyes DC, Alonso JM, Davis KR, Ecker JR, Jones AM (2003) The β-subunit of the *Arabidopsis* G protein negatively regulates auxin-induced cell division and affects multiple developmental processes. Plant Cell **15:** 393–409

Ullah H, Chen JG, Wang S, Jones AM (2002) Role of a heterotrimeric G protein in regulation of Arabidopsis seed germination. Plant Physiol **129:** 897–907

Ullah H, Chen JG, Young JC, Im KH, Sussman MR, Jones AM (2001) Modulation of cell proliferation by heterotrimeric G protein in Arabidopsis. Science **292:** 2066–2069

Urano D, Chen JG, Botella JR, Jones AM (2013) Heterotrimeric G protein signalling in the plant kingdom. Open Biol **3:** 120186

Urano D, Jones AM (2014) Heterotrimeric G protein-coupled signaling in plants. Annu Rev Plant Biol **65:** 365–384

Vuralhan Z, Morais MA, Tai SL, Piper MDW, Pronk JT (2003) Identification and characterization of phenylpyruvate decarboxylase genes in Saccharomyces cerevisiae. Appl Environ Microbiol **69:** 4534–4541

Wang H, Chen H, Hao G, Yang B, Feng Y, Wang Y, Feng L, Zhao J, Song Y, Zhang H, et al (2013) Role of the phenylalanine-hydroxylating system in aromatic substance degradation and lipid metabolism in the oleaginous fungus Mortierella alpina. Appl Environ Microbiol **79:** 3225–3233

Warpeha KM, Gibbons J, Carol A, Slusser J, Tree R, Durham W, Kaufman LS (2008) Adequate phenylalanine synthesis mediated by G protein is critical for protection from UV radiation damage in young etiolated Arabidopsis thaliana seedlings. Plant Cell Environ **31:** 1756–1770

Warpeha KM, Lateef SS, Lapik Y, Anderson M, Lee BS, Kaufman LS (2006) G-protein-coupled receptor 1, G-protein Gα-subunit 1, and prephenate dehydratase 1 are required for blue light-induced production of phenylalanine in etiolated Arabidopsis. Plant Physiol **140:** 844–855

Warpeha KM, Montgomery BL (2016) Light and hormone interactions in the seed-to-seedling transition. Environ Exp Bot **121:** 56–65

Wellesen K, Durst F, Pinot F, Benveniste I, Nettesheim K, Wisman E, Steiner-Lange S, Saedler H, Yephremov A (2001) Functional analysis of the LACERATA gene of Arabidopsis provides evidence for different roles of fatty acid omega-hydroxylation in development. Proc Natl Acad Sci USA **98:** 9694–9699

Wheeler GL, Jones MA, Smirnoff N (1998) The biosynthetic pathway of vitamin C in higher plants. Nature **393:** 365–369

Wituszyńska W, Karpiński S (2013) Programmed cell death as a response to high light, UV and drought stress in plants. Chapter 7. InTech Open doi/10.5772/53127

Xia Y, Yu K, Navarre D, Seebold K, Kachroo A, Kachroo P (2010) The *glabra1* mutation affects cuticle formation and plant responses to microbes. Plant Physiol **154:** 833–846

Yeats TH, Rose JKC (2013) The formation and function of plant cuticles. Plant Physiol **163:** 5–20

Yephremov A, Wisman E, Huijser P, Huijser C, Wellesen K, Saedler H (1999) Characterization of the FIDDLEHEAD gene of *Arabidopsis* reveals a link between adhesion response and cell differentiation in the epidermis. Plant Cell **11:** 2187–2201

Yoo H, Widhalm JR, Qian Y, Maeda H, Cooper BR, Jannasch AS, Gonda I, Lewinsohn E, Rhodes D, Dudareva N (2013) An alternative pathway contributes to phenylalanine biosynthesis in plants via a cytosolic tyrosine:phenylpyruvate aminotransferase. Nat Commun **4:** 2833

Zhang L, Hu G, Cheng Y, Huang J (2008) Heterotrimeric G protein alpha and beta subunits antagonistically modulate stomatal density in Arabidopsis thaliana. Dev Biol **324:** 68–75